Motion Control of a Flock of 1-Trailer Robots with Swarm Avoidance

Jai Raj†*⬥, Krishna Raghuwaiya‡, Bibhya Sharma†⬥ and Jito Vanualailai†

†*School of Computing, Information & Mathematical Sciences, The University of the South Pacific, Suva, Fiji*
E-mails: bibhya.sharma@usp.ac.fj, vanualailai@usp.ac.fj
‡*School of Education, The University of the South Pacific, Suva, Fiji*
E-mail: krishna.raghuwaiya@usp.ac.fj

SUMMARY
This paper addresses the motion planning and control problem of a system of 1-trailer robots navigating a dynamic environment cluttered with obstacles including a swarm of boids. A set of nonlinear continuous control laws is proposed via the Lyapunov-based Control Scheme for collision, obstacle, and swarm avoidances. Additionally, a leader–follower strategy is utilized to allow the flock to split and rejoin when approaching obstacles. The effectiveness of the control laws is demonstrated through numerical simulations, which show the split and rejoin maneuvers by the flock when avoiding obstacles while the swarm exhibits emergent behaviors.

KEYWORDS: Tractor–trailer; Collision avoidance; Unmanned vehicles; Swarm; Motion control; Lyapunov-based Control Scheme.

1. Introduction
The autonomous navigation and control of unmanned vehicles is currently an important research area in robotics involving single or multiple coordinated and connected mobile robots. In essence, connected and autonomous vehicles play a vital role in the transportation industry. Vehicle-to-vehicle (V2V), vehicle-to-infrastructure (V2I), and vehicle-to-everything (V2E) communication ensures connectedness, which is facilitated using wireless and cellular technologies.[1] For instance, the road framework is thought to be well outfitted with sensors and remote advancements to guarantee sufficient correspondence for genuine utilization of the computerized vehicle framework to work. The supposition that is relevant remembering that the current engineering designs for the issue of permitting autonomous vehicles on open roads are pertinent to the advancement of unique paths for streets only for self-driving vehicles instilled with sensors and remote innovations.[2]

The research area has seen a variety of approaches documented in the literature, such as road maps,[3,4] cell decomposition path planning,[5,6] and artificial potential field (APF).[7–12] The differences between the approaches are linked to the type of information about the workspace that is available to the robotic system.[2,13] These differences give rise to the two well-known methods in navigation; *sensor-based method* and *global path planning method*. The sensor-based methods are used when only the local information is available to the robotic system,[14–16] while the global path planning methods are used when the full information on the entire workspace is available to find the optimal path.

The mobile robots are increasingly deployed in real-life applications, such as military-based applications, industrial, office, agriculture automation, search and rescue, surveillance and inspection, to

* Corresponding author. E-mail: jai.raj@usp.ac.fj

name but a few.[8,9,11,12] In essence, mobile robots are tasked with work that could be defined as "dull, dirty, or dangerous".[9,12] Multi-agent robotic systems are more favored in accomplishing specific control objectives as a direct consequence of their effectiveness with the coupling of inherent constraints and restrictions, robustness, flexibility, redundancy, their wide-ranging capabilities, and the abundance of real-world applications compared to a single agent.[9,17–19] The fundamental problem in the motion planning and control of such cooperative systems is finding a collision-free trajectory in environment cluttered with static and dynamic obstacles. The environment is either known or unknown to the cooperative system, hence the control mechanism for safe navigation among obstacles is a problem that still represents a real challenge.[9,11,20]

The performance of multi-agent systems are optimized these days using the autonomous unmanned robots, which can be grouped into four classes: land (ground mobile robots), aquatic (underwater unmanned vehicles), surface vessels, and unmanned aerial vehicles.[21] In this research, our interest lies with the land-dwelling robots, which represent one the largest classes in the four groups. Even though there are various kinds of land robots, wheeled and tracked robots are the most popular because of their workability and simplicity.[9] However, they are difficult to control because the ground contact inflicts a kinematic constraint known as the nonholonomic constraint. This constraint prevents any motion of the wheels in the direction perpendicular to the wheels velocity.[22] The models for the ground mobile robots fall under two categories, namely *dynamic* and *kinematic* model. Dynamic models are based on resolution of physical forces, whereas kinematic models are based on abstracted control inputs. The kinematic model of ground vehicles can be generally categorized into three types – *holonomic*, *unicycle*, and *bicycle*.[21] The differences between the kinematic models are characterized by the different kinematic constraints that are imposed on the models.

1.1. Related works

There are many approaches in literature in relation to the formation control of robots that are developed by either behavioral-based,[17,23] virtual structure,[24] or leader–follower approach.[1,2,8,25,26] The leader–follower technique is most widely used and is well recognized due to its simplicity and reliability. In the leader–follower formation strategy, one mobile robot is designated as the leader and other robots are called followers.[25] The leader will navigate toward its defined target, while the ghost targets normally move relative to the leaders position and the follower robots move toward their designated ghost targets. Formation control of multi-agent systems has been studied effectively with region constraint in ref. [27], obstacle avoidance in refs. [28,29], connectivity preservation and event-triggered controllers in ref. [30], and Lyapunov-based method with obstacle avoidance in refs. [1, 8–10, 12, 31, 32]. Tractor–trailer systems, which are formed by connecting the car-like mobile robot to trailers are used to enhance the performance in autonomous transportation. The foremost inspiration in the research on formation control for a flock of tractor–trailer robots is the increase of transportation volume in a cost-effective way in load carriage, crop harvesting, material collecting, delivery system, and logistical cooperation.[18,33–35]

Many researchers have studied tractor-trailer systems with an on-axle hitching, but only a few have focused on the off-axle hitched trailer system[36] due to its kinematic structure, which is highly complicated. As such, the coupling between the tractor and trailer increases the nonlinearity and complexity of kinematic equations and compound the difficulty in the analysis and controller design. There have been a significant amount of work done to address the motion control of tractor-trailer systems. For example, Divelbiss and Wen in ref. [37] used a front wheel drive tractor to derive the kinematic model for the general *n*-trailer to solve the nonholonomic motion planning problem. In ref. [38], Bolzern et al. proposed control laws for the off-axle hitched trailer system based on linearization of a virtual on-axle vehicle, which shared some properties with the actual one. In ref. [39], Lee et al. presented experimental data for the design and control of passive multiple trailer systems, both off and on-axle. Motion planning and collision avoidance schemes were considered by minimizing the trajectory tracking error with the reference trajectory implying the trajectory of the towing vehicle. In ref. [40], Kayacan and Saeys addressed the robust trajectory tracking error model-based predictive control of tractor–trailer systems. In ref. [41], Ding *et al.* proposed control algorithms for active trailer steering systems using Fuzzy Logic Control and Linear Quadratic Regulator techniques, Astolfi et al. in ref. [42] solved the problem of asymptotic stabilization for straight and circular forward/backward motions using the Lyapunov-based approach, while

Raghuwaiya et al.[1] discussed rigid formation control of the 1-trailer robots. Other very exciting work on tractor–trailer vehicles can be found in refs. [43–45].

This research paper considers a communication system comprising of a flock of tractor–trailer robots navigating amidst a swarm of boids with emergent behaviors, exemplifying V2V and V2I communication system. The tractor–trailer system is a mobile robot composed of a car-like tractor robot, which pulls a number of trailers connected by revolute joints which satisfy nonholonomic constraints. The reader is referred to refs. [20, 22] for a detailed account of nonholonomy.

1.2. Contributions
The main contributions of this research paper are expressed as follows:

1. A new dynamic environment which includes a swarm of boids as moving obstacles, adding a new dimension to the motion planning and control problem. Previous work by the authors involved the motion control of cooperative systems of tractor–trailers while maintaining locally rigid formation in the presence of disk-shaped obstacles;[1]
2. The formation control of a flock of 1-trailer systems with swarm, obstacle, and collision avoidance through a leader–follower strategy with followers having ghost targets. The avoidance of the tractor–trailer system by the swarm of boids, ensuring collision avoidance is a new addition to the control problem. Fixed disk-shaped obstacles and moving robots, which themselves become a moving obstacle to all the other mobile robots in the workspace has been studied,[9,46,47] however, swarm avoidance with tractor–trailer system will be the first of its kind;
3. A closed and bounded workspace as fixed obstacles so that the tractor–trailer robotic system uses the V2I and V2E communication for safe navigation.
4. A simple and elegant method of converting complex dynamical and kinematical constraints into APF functions of the 1-trailer systems. The Lyapunov-based Control Scheme (LbCS) provides a very simple yet an effective way of constructing mathematical functions from limitations, inequalities, restrictions, and mechanical constraints tagged to the mechanical systems into APF functions, and subsequently incorporate these into the controllers derived from LbCS. Other motion planning and control schemes available in the literature find much difficulty in incorporating these limitations into their control laws when compared to the LbCS;[9,26,48]
5. A unified set of nonlinear, time-invariant acceleration-based control laws for a heterogeneous robotic system that is efficiently designed at the kinematic level via LbCS.

The remainder of this paper is structured as follows: in Section 2, the kinematic model of the 1-trailer system and the swarm model are briefly presented; in Section 3, the objectives of the research is outlined; in Section 4, the APF functions are defined under the influence of kinodynamic constraints; in Section 5, the Lyapunov function is introduced including the controller design; in Section 6, the stability analysis of the robotic system is carried out; in Section 7, we demonstrate the effectiveness of the proposed controllers via numerical simulations; and finally, Section 8 concludes the paper and outlines future work in the area.

2. System Architecture
In this section, we shall model a tractor–trailer system and a swarm of disk-shaped boids using planar Cartesian coordinates. The steerable standard 1-trailer system and swarm of boids will be used to design a kinodynamic system in a bounded yet dynamic environment.

2.1. The 1-trailer system model
There are two different trailer systems, namely the standard and general trailer systems. The different hooking mechanism schemes classify the two different categories of the trailer systems.[49] In this research, the steerable *standard* 1-trailer system will be considered, which is a car-like mobile robot attached to a two-wheeled active trailer. A schematic diagram is represented in Fig. 1. A revolute link or a rigid bar of length L_{i1} and L_{i2} joins the two vehicles; from the midpoint of the rear axle of the ith vehicle to the midpoint of the rear axle of the ith trailer. The connections between the two bodies
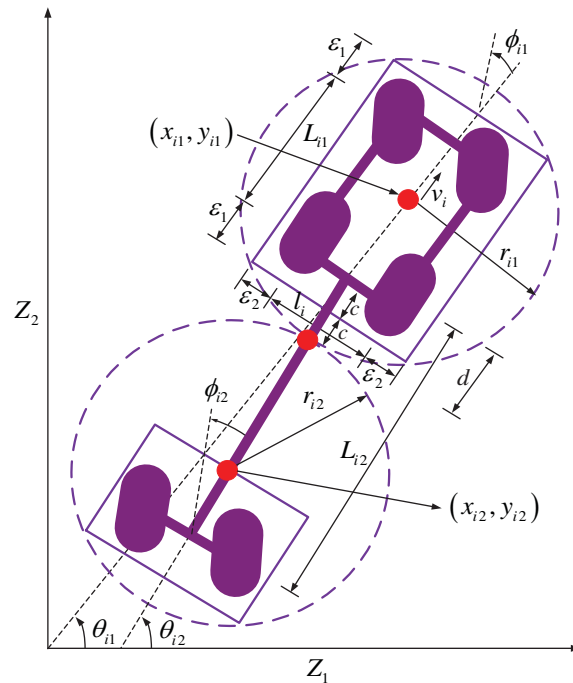
Fig. 1. The kinematic model of $\mathcal{A}_i$, a rear-wheel-driven steerable standard 1-trailer system with front-wheel steering and steering angle, ϕ_{i1} and one on-axle hitched two-wheeled active trailer in the Euclidean plane.

give rise to the following nonholonomic constraints on the system, which in general is the position of the attached trailer, adopted from ref. [25]:

$$x_{i2} = x_{i1} - \frac{L_{i1}}{2} \cos \theta_{i1} - \frac{L_{i2} + 2d}{2} \cos \theta_{i2}, \quad y_{i2} = y_{i1} - \frac{L_{i1}}{2} \sin \theta_{i1} - \frac{L_{i2} + 2d}{2} \sin \theta_{i2}, \quad (1)$$

for $i = i, \ldots, n$. These constraints will reduce the dimension of the configuration space. In addition, we assume that there is no slippage of the rear and the front wheels of the tractor of the 1-trailer system, that is, the lateral velocities of the wheels of the tractor are assumed to be zero. We begin with the following definition:

Definition 1. *The ith nonholonomic steerable standard 1-trailer system, $i = 1, \ldots, n$, $n \in \mathbb{N}$, comprises of two disks. The first disk, centered at (x_{i1}, y_{i1}) with radius r_{i1}, represents the rear-wheel driven and front-wheel steered car-like vehicle, defined precisely as*

$$\mathcal{A}_{i1} := \{(z_1, z_2) \in \mathbb{R}^2 : (z_1 - x_{i1})^2 + (z_2 - y_{i1})^2 \leq r_{i1}^2\}.$$

The second disk, centered at (x_{i2}, y_{i2}) with radius r_{i2}, represents the on-axle hitched two-wheeled active trailer, defined precisely as

$$\mathcal{A}_{i2} := \{(z_1, z_2) \in \mathbb{R}^2 : (z_1 - x_{i2})^2 + (z_2 - y_{i2})^2 \leq r_{i2}^2\}.$$

Then the ith steerable standard 1-trailer system is the set

$$\mathcal{A}_i := \mathcal{A}_{i1} \cup \mathcal{A}_{i2}.$$

With reference to Fig. 1, (x_{im}, y_{im}), $i = 1, \ldots, n$, and $m = 1, 2$, is the reference point of each solid body of the articulated robot, θ_{im} gives the orientation of the mth body of $\mathcal{A}_i$ with respect to the z_1-axis of the $z_1 z_2$-plane. Moreover, ϕ_{im} gives the steering angle of the mth body of $\mathcal{A}_i$ with respect to its longitudinal axis. For simplicity, we assume that the dimensions of the robots are kept the same. Therefore, L_{i1} is the distance between the centers of the front and rear axles of $\mathcal{A}_i$'s tractor, L_{i2} is the distance between the centers of the front and rear axles of the attached trailer, and l_i is the length of each axle. If we let m_i be the mass of the full robot, F_i is the force along the axis of the tractor–trailer robot, Γ_{i1} and Γ_{i2} are the torque about a vertical axis at (x_0, y_0), and I_{i1} and I_{i2} are the moment

of inertia of the tractor–trailer robot, then the dynamic model of $\mathcal{A}_i$, adopted from ref. [49], is then derived as

$$
\left.
\begin{aligned}
\dot{x}_{i1} &:= v_i \cos \theta_{i1} - \tfrac{L_{i1}}{2} \omega_{i1} \sin \theta_{i1}, \\
\dot{y}_{i1} &:= v_i \sin \theta_{i1} + \tfrac{L_{i1}}{2} \omega_{i1} \cos \theta_{i1}, \\
\dot{\theta}_{i1} &:= \tfrac{v_i}{L_{i1}} \tan \phi_{i1} =: \omega_{i1}, \\
\dot{\theta}_{i2} &:= \tfrac{v_i}{L_{i2}} \sin(\theta_{i1} - \theta_{i2}) =: \omega_{i2}, \\
\dot{v}_i &:= \tfrac{F_i}{m_i} = \sigma_{i1}, \\
\dot{\omega}_{i1} &:= \tfrac{\Gamma_{i1}}{I_{i1}} = \sigma_{i2}, \qquad \dot{\omega}_{i2} := \tfrac{\Gamma_{i2}}{I_{i2}} = \sigma_{i3},
\end{aligned}
\right\}
\tag{2}
$$

for $i = 1, \ldots, n$. Note that v_i and ω_{i1} are, respectively, the instantaneous translational and rotational velocities, while σ_{i1} and σ_{i2} are, respectively, the instantaneous translational and rotational accelerations of the tractor of $\mathcal{A}_i$, whereas ω_{i2} and σ_{i3} are, respectively, the instantaneous rotational velocity and the instantaneous rotational acceleration of $\mathcal{A}_i$'s trailer. Moreover, without any loss of generality, we assume that $\phi_{im} = \theta_{im}$. The state space of $\mathcal{A}_i$ is then illustrated by $\mathbf{x}_i := (x_{i1}, y_{i1}, \theta_{i1}, \theta_{i2}, v_i, \omega_{i1}, \omega_{i2}) \in \mathbb{R}^7$, for $i = 1, 2, \ldots, n$. For the n members constituting the flock of the steerable 1-trailer systems, we further define $\mathbf{x} := (\mathbf{x}_1, \mathbf{x}_2, \ldots, \mathbf{x}_n) \in \mathbb{R}^{7n}$.

Furthermore, to ensure that the entire vehicle safely steers pass an obstacle, the planar vehicle can be represented as a simpler fixed-shaped object, such as a circle, a polygon, or a convex hull.[2,9,33] This representation is facilitated with the view of minimizing the obstacle space (C-space) in the workspace. We enclose each body of the articulated vehicle within two separate protective circular regions (as seen in Fig. 1), which basically reduces the unnecessary growth of the C-space. Hence, to ensure that each articulated body of $\mathcal{A}_i$ safely steers past an obstacle, given $d := \varepsilon_1 + c$ and *clearance parameters* $\varepsilon_1 > 0$ and $\varepsilon_2 > 0$, we enclose the first body of $\mathcal{A}_i$, that is the tractor, by a protective circular region centered at (x_{i1}, y_{i1}), with radius $r_{i1} := \sqrt{(L_{i1} + 2\varepsilon_1)^2 + (l_i + 2\varepsilon_2)^2}/2 = (L_{i1} + 2d)/2$. Similarly, for the second body of $\mathcal{A}_i$, that is the trailer, enclosure is again with a circular protective region centered at (x_{i2}, y_{i2}) with radius $r_{i2} := \sqrt{(L_{i2} - 2c)^2 + (l_i + 2\varepsilon_2)^2}/2$.

2.2. A swarm model

Biological systems such as the groups of fish, ants, birds, and bacteria reveal some amazing cooperative behaviors while in motion. These cooperative behaviors can be classified as separation, alignment, and cohesion. They describe how each member or boid, maneuvers, based on the positions and velocities of its nearby flockmates.[50]

We shall construct a model of a swarm with h individuals moving with the velocity of the swarm's centroid. Following the nomenclature of Reynolds,[50] each member of the flock is denoted as a boid. A general swarm model, formulated by Mogilner et al.[51] will be utilized. We begin with the following definition for the swarm model:

Definition 2. *A swarm is a collection of a large number of individuals, called* boids. *At time $t \geq 0$, let $(xb_k(t), yb_k(t))$, $k = 1, \ldots, h$, $h \in \mathbb{N}$, be the planar position of the kth individual, which we shall define as a boid residing in a disk of radius $rb_k \geq 0$,*

$$
\mathcal{B}_k := \left\{ (z_1, z_2) \in \mathbb{R}^2 : (z_1 - xb_k)^2 + (z_2 - yb_k)^2 \leq rb_k^2 \right\}.
\tag{3}
$$

The disk is described in ref. [51] as a *bin* and in ref. [52] as a *private or safety area*, of each individual. We shall use the former term, with *bin size* being the radius rb_k of the disk.

Let us define the *centroid of the swarm* as

$$
(xb_C, yb_C) := \left(\frac{1}{h} \sum_{k=1}^{h} xb_k, \frac{1}{h} \sum_{k=1}^{h} yb_k \right).
\tag{4}
$$

At time $t \geq 0$, let $(\upsilon b_k(t), \omega b_k(t) := (\dot{xb}_k(t), \dot{yb}_k(t)))$ be the instantaneous velocity of the kth boid. Using the above notations, a system of first order ODE's for the kth boid is obtained, assuming the initial conditions at $t = t_0 \geq 0$:

$$\left.\begin{aligned} \dot{xb}_k &= \upsilon b_k(t), \\ \dot{yb}_k &= \omega b_k(t), \\ xb_{k0} &:= xb_k(t_0), \ \ yb_{k0} := yb_k(t_0), \ \ k = 1, \ldots, h, \ h \in \mathbb{N}. \end{aligned}\right\} \quad (5)$$

Suppressing t, let $\mathbf{x}_k = (xb_k, yb_k) \in \mathbb{R}^2$ and $\mathbf{x} = (\mathbf{x}_1, \ldots, \mathbf{x}_n) \in \mathbb{R}^{2n}$ be the state vectors. Also, let

$$\mathbf{x}_0 = \mathbf{x}(t_0) = (xb_{10}, yb_{10}, \ldots, xb_{n0}, yb_{n0}).$$

If $\mathbf{g}_k(\mathbf{x}) := (\upsilon b_k, \omega b_k) \in \mathbb{R}^2$ and $\mathbf{G}(\mathbf{x}) := (\mathbf{g}_1(\mathbf{x}), \ldots, \mathbf{g}_n(\mathbf{x})) \in \mathbb{R}^{2n}$, then the swarm system of h boids is

$$\dot{\mathbf{x}} = \mathbf{G}(\mathbf{x}), \ \ \mathbf{x}_0 = \mathbf{x}(t_0), \ \ t_0 \geq 0. \quad (6)$$

2.3. Heterogeneous system: 1-trailer and swarm

The combined dynamic model of the steerable 1-trailer system and the swarm of boids is given by

$$\left.\begin{aligned} \dot{x}_{i1} &= v_i \cos \theta_{i1} - \frac{L_{i1}}{2}\omega_{i1} \sin \theta_{i1} , \\ \dot{y}_{i1} &= v_i \sin \theta_{i1} + \frac{L_{i1}}{2}\omega_{i1} \cos \theta_{i1} , \\ \dot{\theta}_{i1} &= \frac{v_i}{L_{i1}} \tan \phi_{i1} =: \omega_{i1} , \\ \dot{\theta}_{i2} &= \frac{v_i}{L_{i2}} \sin (\theta_{i1} - \theta_{i2}) = \omega_{i2} , \\ \dot{v}_i &= \frac{F_i}{m_i} = \sigma_{i1}, \\ \dot{\omega}_{i1} &= \frac{\Gamma_{i1}}{I_{i1}} = \sigma_{i2}, \qquad \dot{\omega}_{i2} = \frac{\Gamma_{i2}}{I_{i2}} = \sigma_{i3}, \\ \dot{xb}_k &= \upsilon b_k, \qquad\qquad \dot{yb}_k = \omega b_k , \end{aligned}\right\} \quad (7)$$

for $i = 1, \ldots, n$ and $k = 1, \ldots, h$. This forms the model of the dynamic team and to the authors knowledge, it is the first time that such a dynamic team consisting of the tractor–trailer pair and the swarm of boids is being modeled together for a formation control problem.

3. Research Objective

Given *a priori-known* environment in the $z_1 z_2$-plane cluttered with obstacles, our objective is to design nonlinear time-invariant controllers σ_{i1}, σ_{i2}, and σ_{i3} to facilitate the movement of a team of 1-trailer system from an initial configuration to its final target while ensuring swarm, obstacle, and collision avoidances. The different types of avoidance in this heterogeneous system will arise from the following:

1. disk-shaped fixed obstacles;
2. inter-1-trailer system;
3. intra-swarm;
4. artificial obstacles constructed from dynamic constraints; and
5. swarm of boids.

4. Artificial Potential Field Functions

This section formulates collision-free trajectories of the robotic system under kinodynamic constraints in a fixed and bounded workspace using APF method. The principle idea that governs the
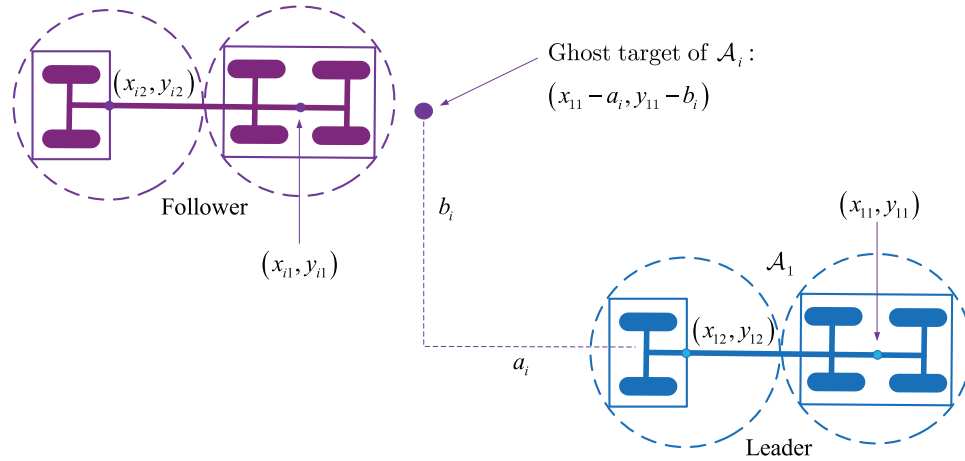
Fig. 2. Positioning of the mobile ghost targets of $\mathcal{A}_i$ for $i = 2, \ldots, n$, relative to the leader $\mathcal{A}_1$.

APF method is finding a function that represents the energy of the system, such as the Lyapunov function and generating a force so that the energy of the system is minimized and reach the minimum value, preferably only at the goal configuration. The energy of the system is mathematically treated as the total potential. It is assumed that each $\mathcal{A}_i$ and $\mathcal{B}_k$ has a *a priori* knowledge of the entire workspace. We design the acceleration-based controllers, σ_{i1}, σ_{i2}, and σ_{i3}, such that the flock of 1-trailer system will navigate safely in the workspace and reach a neighborhood of its target. To obtain a feasible solution, we utilize APF functions via the LbCS to design new controllers. We begin by describing precisely the target, the workspace, and all obstacles.

4.1. Attractive potential field functions for the 1-trailer systems
4.1.1. Attraction to the target of the tractor–trailer pair.
The leader–follower scheme is utilized for the establishment and advancement of the flock of n robot 1-trailer systems. A target is assigned to the leader of the articulated leader robot $\mathcal{A}_1$ to reach after some time t, which initiates the movement of the vehicular system. An attractive force needs to be established between the leader robot $\mathcal{A}_1$ and the follower robots $\mathcal{A}_i$, $i = 2, \ldots, n$ via the leader–follower scheme to enable the follower robots to follow $\mathcal{A}_1$ via the concept of mobile ghost targets,[1] as illustrated in Fig. 2. Essentially, we require $\mathcal{A}_1$ to start from an initial position, move toward its designated target and finally converge at the center of its designated target, while the follower robots follow $\mathcal{A}_1$ in accordance to the leader–follower scheme.

Definition 3. *The stationary target T_i for $\mathcal{A}_i$ is a circular disk with center (p_{i1}, p_{i2}) and radius rp_i for $i = 1, \ldots, n$, defined by the set*

$$T_i := \left\{ (z_1, z_2) \in \mathbb{R}^2 : (z_1 - p_{i1})^2 + (z_2 - p_{i2})^2 \leq rp_i^2 \right\}.$$

In the leader–follower scheme, the leader robot $\mathcal{A}_1$ will move toward its designated target with center (p_{11}, p_{12}), while the ghost targets move relative to the leader's position and the follower robots $\mathcal{A}_i$, $i = 2, \ldots, n$ move toward their designated ghost targets.[1] The mobile ghost target for the ith follower robot is positioned relative to the position of $\mathcal{A}_1$, with center given as $(p_{i1}, p_{i2}) = (x_{11} - a_i, y_{11} - b_i)$, for $a_i, b_i \in \mathbb{R}$ and $i = 2, \ldots, n$. Hence, for the attraction of $\mathcal{A}_i$ to its designated/ghost target, we consider an attractive potential function of the form

$$V_i(\mathbf{x}) := \frac{1}{2} \left[(x_{i1} - p_{i1})^2 + (y_{i1} - p_{i2})^2 + v_i^2 + \sum_{m=1}^{2} \omega_{im}^2 \right], \tag{8}$$

for $i = 1, \ldots, n$. The above function is not only a measure of the Euclidean distance between the center of $\mathcal{A}_i$ and its target but also a measure of its convergence to the target with the inclusion of the translational and rotational velocities. At the target center (p_{i1}, p_{i2}), we desire the velocities, v_i and ω_{im} to be zero to ensure that the tractor–trailer pairs stop. The 1-trailer robots will move toward the target which is a local minima. We define $\mathbf{x}^* := (p_{01}, p_{02}, 0, 0) \in \mathbb{R}^4$, then we see that
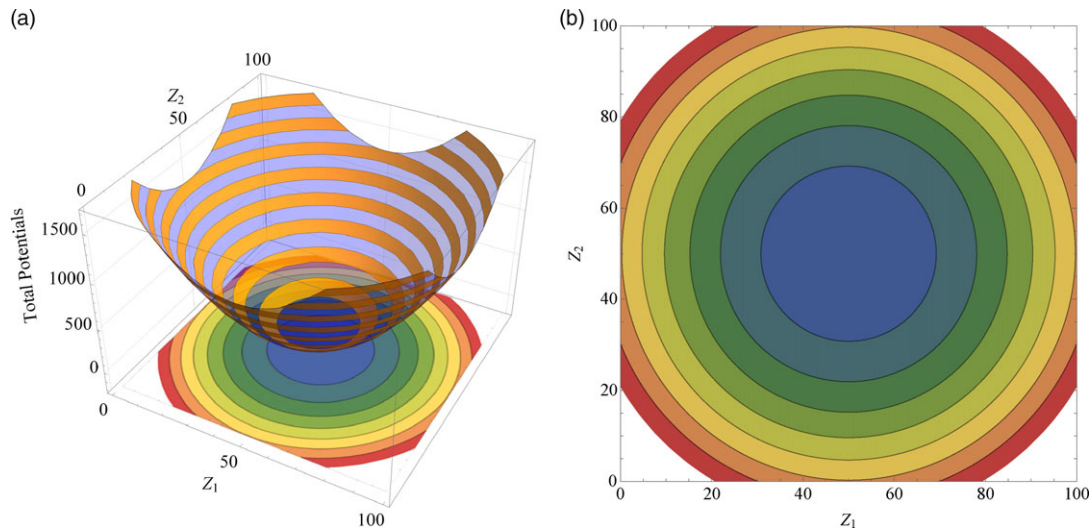
Fig. 3. The attractive potential fields and the corresponding contour plot generated using the target attractive function, Eq. (8). The dimensions of the 1-trailer system are given in Table I, while $v_0 = 5$ and ω_{01}, $\omega_{02} = \pi/4$. The disk-shaped target for the tractor robot is fixed at $(p_{01}, p_{02}) = (50, 50)$ with a radius of $rp_0 = 1$. For this case, we are considering a single 1-trailer system. (a) 3D visualization. (b) Contour plot.

$V_i(\mathbf{x}^*) = 0$. This is an implication that the role of $V_i(\mathbf{x})$ in the Lyapunov function is to ensure that system trajectories start and remain close to $\mathbf{x}^*$, forcing $\mathbf{x}^*$, via the controllers, to be an equilibrium point of system (7). In other words, if the 1-trailer system ever converges to its target, then it remains there at all times.

An illustration of the total potentials for the target attraction function is shown in Fig. 3(a), while Fig. 3(b) shows the corresponding contour plot generated over a workspace $0 < z_1 < 100$ and $0 < z_2 < 100$ for the articulated robot.

4.1.2. Auxiliary function. To guarantee the convergence of $\mathcal{A}_i$ to its designated target and ensure that the nonlinear controllers vanish at the target configuration, we consider the auxiliary function of the form

$$G_i(\mathbf{x}) := \frac{1}{2}\left[(x_{i1} - p_{i1})^2 + (y_{i1} - p_{i2})^2\right], \tag{9}$$

for $i = 1, \ldots, n$. This auxiliary function is then multiplied to the inverse of each of the repulsive potential field functions to be designed in the following subsections.

4.2. Repulsive potential field functions for the 1-trailer system
We want the members of the flock of 1-trailer system to avoid all obstacles intersecting their paths. The fixed obstacles are the *four* boundaries of the rectangular workspace of the tractor–trailer pair, and the stationary solid objects fixed within the workspace. On the other hand, the moving obstacles consist of the flock of 1-trailer systems and the swarm of boids. The artificial obstacles are created to satisfy the dynamic constraints of the system. Hence, we construct obstacle avoidance functions that measure the Euclidean distances between each articulated body of $\mathcal{A}_i$ and the obstacles in the workspace.

4.2.1. Fixed obstacles. V2I communication is used for the flock of tractor–trailer pairs to avoid all the fixed obstacles. For the avoidance of this obstacles, we design an obstacle avoidance function. Let us fix $l \in \mathbb{N}$ solid obstacles within the boundaries of the workspace.

Definition 4. *A stationary solid object is a disk with center (o_{l1}, o_{l2}) and radius ro_l. Precisely, the solid object is the set*

$$O_l := \left\{(z_1, z_2) \in \mathbb{R}^2 : (z_1 - o_{l1})^2 + (z_2 - o_{l2})^2 \leqslant ro_l^2\right\}.$$

For its avoidance by $\mathcal{A}_i$, we consider the obstacle avoidance function

$$FO_{iml}(\mathbf{x}) := \frac{1}{2} \left[(x_{im} - o_{l1})^2 + (y_{im} - o_{l2})^2 - (ro_l + r_{im})^2 \right], \tag{10}$$

where $i = 1, \ldots, n$, $m = 1, 2$, and $l = 1, \ldots, q$.

These dynamic constraints can be factored within the motion planners and control schemes of the 1-trailer system by constructing *artificial obstacles* and then avoiding them to achieve the desired outcome which when coupled together with *tuning parameters*, will appear in the denominator of the Lyapunov function as per the requirements of the LbCS. For each the repulsive potential field functions that will be created, the same approach will be considered.

4.2.2. Dynamic constraints and modulus bound on velocities. The translational velocity is limited for safety reasons, while the rotational velocity is limited as a result of inherent constraints on $\mathcal{A}_i$. Hence, we include the following additional constraints:

1. $|v_i| < v_{\max}$, where $v_{\max}$ is the *maximum achievable speed* of $\mathcal{A}_i$;

2. $|\omega_{i1}| < \dfrac{v_{\max}}{|\rho_{\min}|}$, where $\rho_{\min} := \dfrac{L_{i1}}{\tan(\phi_{\max})}$. This is derived from the fact that $|\phi_{i1}| \leq \phi_{\max}$, where $\phi_{\max}$ is the *maximum steering angle*. This condition is attributed to the boundedness of the steering angle ϕ_{i1};

3. $|\omega_{i2}| < \dfrac{v_{\max}}{L_{i2}} =: \omega_{2\,\max}$, where $\omega_{2\,\max}$ is the *maximum rotational velocity* of the trailer;

4. $|\theta_{i1} - \theta_{i2}| \leq \theta_{\max} < \dfrac{\pi}{2}$, where $\theta_{\max}$ is the *maximum bending angle* of the trailer with respect to the orientation of the tractor. In essence, the trailer is free to rotate within $\left(-\frac{\pi}{2}, \frac{\pi}{2}\right)$, hence circumventing a *jack knife* situation.

Remark 1. For simplicity, the values of $v_{\max}$, $\phi_{\max}$, and $\theta_{\max}$ will be kept the same for each mobile robot, $\mathcal{A}_i$.

For each of the dynamic constraints, we construct a corresponding artificial obstacle:

$$AO_{i1} := \{ v_i \in \mathbb{R} : v_i \leq v_{\max} \}, \qquad AO_{i2} := \{ \omega_{i1} \in \mathbb{R} : \omega_{i1} \leq -v_{\max}/\rho_{\min} \},$$
$$AO_{i3} := \{ \omega_{i2} \in \mathbb{R} : \omega_{i2} \leq -v_{\max}/L_{i2} \}, \qquad AO_{i4} := \{ (\theta_{i1}, \theta_{i2}) \in \mathbb{R} : (\theta_{i1} - \theta_{i2}) \leq -\theta_{\max} \}.$$

Figure 4 outlines the representation of the artificial obstacle got from the constraint on the translational speed of a robot. For the avoidance of these artificial obstacles, we construct the following obstacle avoidance functions:

$$\left.\begin{aligned}
DC_{i1}(\mathbf{x}) &:= \frac{1}{2} \left(v_{\max} - v_i \right) \left(v_{\max} + v_i \right), \\
DC_{i2}(\mathbf{x}) &:= \frac{1}{2} \left(\frac{v_{\max}}{|\rho_{\min}|} - \omega_{i1} \right) \left(\frac{v_{\max}}{|\rho_{\min}|} + \omega_{i1} \right), \\
DC_{i3}(\mathbf{x}) &:= \frac{1}{2} \left(\omega_{2\,\max} - \omega_{i2} \right) \left(\omega_{2\,\max} + \omega_{i2} \right), \\
DC_{i4}(\mathbf{x}) &:= \frac{1}{2} \left(\theta_{\max} - (\theta_{i2} - \theta_{i1}) \right) \left(\theta_{\max} + (\theta_{i2} - \theta_{i1}) \right),
\end{aligned}\right\} \tag{11}$$

for $i = 1, \ldots, n$. These positive functions would guarantee the adherence to the limitations imposed upon the steering angle and the velocities of $\mathcal{A}_i$.

4.2.3. Workspace limitations. We want to setup a simple framework for the workspace of our robotic system so that the flock of 1-trailer systems is confined to a rectangular region at all time $t \geq 0$. Essentially, the robots motion will be confined to these boundary limitations.
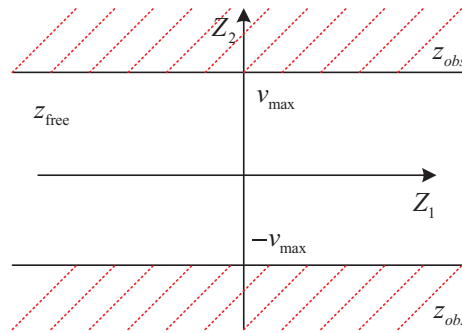
Fig. 4. The obstacle space (z_{obs}) and free space (z_{free}) from the artificial obstacle created for the restriction on the speed of a robot.

Definition 5. *The workspace is a fixed, closed, and bounded rectangular region, defined, for some*

$\eta_b > 2r$ *for* $b = 1, 2$ *with* $r = \sum\limits_{m=1}^{2} r_{im}$, $i = 1, \ldots, n$ *as*

$$WS := \{(z_1, z_2) \in \mathbb{R}^2 : 0 \leq z_1 \leq \eta_1, 0 \leq z_2 \leq \eta_2\}.$$

We require the robotic system to stay within the rectangular region and be avoided at all time $t \geq 0$. Therefore, we impose the following conditions for the *four* boundaries:

Left Boundary : $(z_1, z_2) : z_1 = 0$,   Upper Boundary : $(z_1, z_2) : z_2 = \eta_2 > 0$,

Right Boundary : $(z_1, z_2) : z_1 = \eta_1 > 0$,   Lower Boundary : $(z_1, z_2) : z_2 = 0$.

In the control scheme, these boundaries are considered as *fixed obstacles*, which have to be avoided at all time $t \geq 0$. For the ith body of each robot to avoid these, we define the following potential functions for the left, upper, right, and lower boundaries, respectively:

$$\left.\begin{array}{ll} WT_{im1}(\mathbf{x}) := x_{im} - r_{im}, & WT_{im2}(\mathbf{x}) := \eta_2 - (y_{im} + r_{im}) , \\ WT_{im3}(\mathbf{x}) := \eta_1 - (x_{im} + r_{im}) , & WT_{im4}(\mathbf{x}) := y_{im} - r_{im}, \end{array}\right\} \tag{12}$$

for $i = 1, \ldots, n$ and $m = 1, 2$. Now, since $\eta_b > 2(\sum\limits_{m=1}^{2} r_{im})$, each of the functions is positive in workspace.

As an illustration of the total potential, consider the presence of $l = 3$ obstacles within the workspace bounded by $0 < z_1 < 100$ and $0 < z_2 < 100$. The total potential field function that governs the motion of the leader $\mathcal{A}_1$ is

$$L^* (\mathbf{x}) := V_1 (\mathbf{x}) + G_1 (\mathbf{x}) \left(\sum_{m=1}^{2} \sum_{s=1}^{4} \frac{\tau_{1ms}}{WT_{1ms} (\mathbf{x})} + \sum_{m=1}^{2} \sum_{l=1}^{3} \frac{\alpha_{1ml}}{FO_{1ml} (\mathbf{x})} \right), \tag{13}$$

where τ_{1ms} and α_{1ml} are the control parameters for the workspace and fixed obstacles, respectively. The three-dimensional view of the total potentials and the corresponding contour plot generated by $L^* (\mathbf{x})$ is presented in Fig. 5, essentially the artificial force of $L^* (\mathbf{x})$. The figure shows the attractive potential created by $V_1 (\mathbf{x})$ and repulsive potentials created by $\sum\limits_{m=1}^{2} \sum\limits_{s=1}^{4} \frac{\tau_{1ms}}{WT_{1ms}(\mathbf{x})}$ and $\sum\limits_{m=1}^{2} \sum\limits_{l=1}^{3} \frac{\alpha_{1ml}}{FO_{1ml}(\mathbf{x})}$.

4.2.4. Moving robots. There are two classes of moving obstacles that we will consider in this section: flock of 1-trailer robots and the swarm of boids. We will design an avoidance scheme to avoid the moving obstacles which the system has *a priori* knowledge.

Avoidance of other 1-trailer robots
A moving 1-trailer robot itself becomes a moving obstacle to all the other 1-trailer robots in the workspace. Additionally, each articulated body of the 1-trailer robot has to be treated as a moving
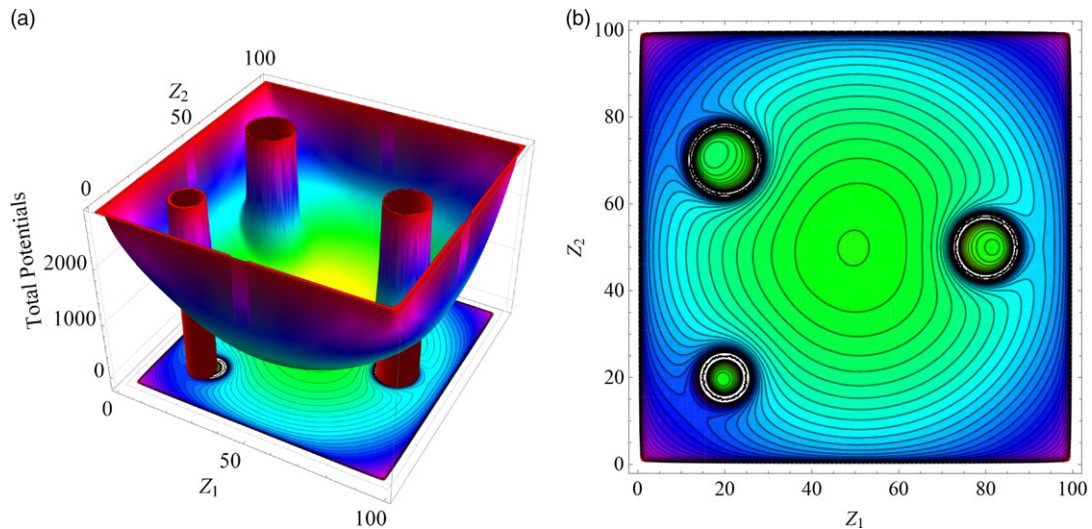
Fig. 5. The total potentials generated for target attraction, workspace limitations, and avoidance of three fixed obstacles governed by $L^*(\mathbf{x})$ (Eq. (13)) and the corresponding contour plot. The target is a disk fixed at $(p_{11}, p_{12}) = (50, 50)$; the obstacles are disk-shaped, fixed at $(o_{11}, o_{12} = 20, 20)$, $(o_{21}, o_{22} = 20, 70)$, and $(o_{31}, o_{32} = 80, 50)$ with radii of $ro_1 = 5$, $ro_2 = 8$, and $ro_3 = 7$, respectively while $\alpha_{1ml} = 500$; and with boundary control parameter as $\tau_{1ms} = 10,000$. In addition, the translational and the angular velocities of the tractor–trailer pair are treated as constants with $v_1 = 1$ and $\omega_{11} = \omega_{12} = \pi/360$, respectively. (a) A three-dimensional visualization of the total potentials. (b) A contour plot of the total potentials.

obstacle for all the other members, via V2V communication. Therefore, for each mth component of $\mathcal{A}_i$ to avoid the uth moving solid body of $\mathcal{A}_j$, we design repulsive potential field function with the associated obstacle avoidance function:

$$MT_{muij}(\mathbf{x}) := \frac{1}{2}\left[(x_{im} - x_{ju})^2 + (y_{im} - y_{ju})^2 - (r_{im} + r_{ju})^2\right],\qquad(14)$$

for $i, j = 1, \ldots, n$, with $j \neq i$ and $m, u = 1, 2$.

Avoidance of swarm of boids
Each member of the flock of 1-trailer robot needs to avoid the swarm of boids again via V2V communication. The avoidance of the swarm of boids is a new addition to the motion planning and control problem. Quintessentially, each boid of the swarm of boids becomes a moving obstacle for the flock of 1-trailer systems in the workspace. Practically, the existence of collision avoidance is pertinent to both the flock of 1-trailer systems and the swarm of boids. However, in this case, we only consider a *one*-way collision avoidance scheme whereby only the flock of 1-trailer systems avoid the swarm of boids, which is achievable via suitable tuning parameters.[9] As such, we design a repulsive potential field function for a one-way obstacle avoidance function:

$$ST_{imk}(\mathbf{x}) := \frac{1}{2}\left[(x_{im} - xb_k)^2 + (y_{im} - yb_k)^2 - (r_{im} + rb_k)^2\right],\qquad(15)$$

for $i = 1, \ldots, n$, $m = 1, 2$, and $k = 1, \ldots, h$. The collision avoidance considered here is for the individual boids and not the whole swarm for the emergent split and rejoin maneuvers.

4.3. *Potential field functions for the swarm of boids*
In this section, we will formulate potential field functions for the swarm of boids that would ensure the attraction of the swarm to the centroid, inter-boid collision and fixed obstacle avoidances.

4.3.1. Attraction to the centroid. Reynolds flocking rules of separation, alignment, and cohesion can be applied to generate or capture cooperative behaviors, which describe how an individual maneuvers based on the positions and velocities of its nearby flock mates.[50,53] Through cohesion, a boid moves toward the center of mass of its neighboring boids; via separation, the boid is moving away from

the nearest boids in order to avoid possible collision; and by alignment, the boid adjusts its heading according to the average heading of those boids in the neighborhood. The superposition of these rules results in the generation of cooperative behavior by the boids moving in a particular formation with a synchronized motion, while ensuring all possible collision and obstacle avoidances. The goal is to ensure that individuals of the swarm are attracted toward each other and form a cohesive group by having a measurement of the distance from the kth individual to the swarm centroid.[54] The rule stipulates that the individuals stay close to the nearest flock mates. Thus, for attraction toward the center of the swarm, we define the following attraction function:

$$R_k(\mathbf{x}) := \frac{1}{2}\left[\left(xb_k - \frac{1}{h}\sum_{a=1}^{h} xb_a\right)^2 + \left(yb_k - \frac{1}{h}\sum_{a=1}^{h} yb_a\right)^2\right]. \tag{16}$$

where $k = 1, \ldots, h$, $k \in \mathbb{N}$. This will be part of the total potentials for the heterogeneous system (7), and its role is to ensure that kth boid is attracted to the swarm centroid.

4.3.2. Avoidance of the workspace boundaries. As discussed in Section 4.2.3, we need to enclose the swarm within the confinement of the workspace since the environment is *priori-known* using V2I communication. We define the avoidance of the four boundaries, namely, left, upper, right and lower boundaries, by the following obstacle avoidance functions:

$$\left. \begin{aligned} WB_{k1}(\mathbf{x}) &:= xb_k - rb_k, & WB_{k2}(\mathbf{x}) &:= \eta_2 - (yb_k + rb_k), \\ WB_{k3}(\mathbf{x}) &:= \eta_1 - (xb_k + rb_k), & WB_{k4}(\mathbf{x}) &:= yb_k - rb_k. \end{aligned} \right\} \tag{17}$$

4.3.3. Intra-swarm collision avoidance. The moving boids themselves become obstacles to the other boids of the swarm. Consequently using the V2V communication, the short range repulsion between individuals necessitates first a measurement of the distance between the kth and the ath individuals, $a \neq k$, $a, k \in \mathbb{N}$. For the boids to avoid each other, we design an obstacle avoidance function:

$$SB_{ka}(\mathbf{x}) := \frac{1}{2}\left[(xb_k - xb_a)^2 + (yb_k - yb_a)^2 - (rb_k + rb_a)^2\right]. \tag{18}$$

The function is an Euclidean measure of the distance between the individual boids, and will appear in the denominator of an appropriate term in the Lyapunov function designed later in the paper.

4.3.4. Avoidance of fixed obstacles by the swarm of boids. The individual boid also need to avoid all the fixed obstacles along its path. Accordingly using the V2I communication, for the avoidance of the fixed obstacles defined in Section 4.2.1 by the kth boid, we consider the following obstacle avoidance function:

$$FB_{kl}(\mathbf{x}) := \frac{1}{2}\left[(xb_k - o_{l1})^2 + (yb_k - o_{l2})^2 - (rb_k + ro_l)^2\right], \tag{19}$$

where $k = 1, \ldots, h$ and $l = 1, \ldots, q$.

4.3.5. Termination of the swarm motion. We want to ensure that the swarm comes to a stop at some point in time. Hence, an auxiliary function governed by Section 4.1.2 is added appropriately to the swarm part of the Lyapunov function to ensure that the swarm stops. This coincides with the situation when robot reach their target.

5. Design of the Nonlinear Controllers
In this section, the nonlinear control laws for system (7) will be designed using the LbCS methodology.

5.1. Lyapunov function
In accordance with the LbCS, we construct the total potentials, that is, the Lyapunov function for system (7) by combining all the attractive and repulsive potential functions. First, for $i = 1, \ldots, n$

and $k = 1, \ldots, h$, we introduce the following *control/tuning parameters* to be utilized in the total potentials:

1. $\alpha_{iml} > 0$, $l = 1, \ldots, q$, $m = 1, 2$ for the collision avoidance of q disk-shaped obstacles (see Section 4.2.1);
2. $\gamma_{is} > 0$, $s = 1, \ldots, 4$, for the avoidance of the sth artificial obstacles from dynamic constraints (see Section 4.2.2);
3. $\tau_{ims} > 0$, $s = 1, \ldots, 4$, $m = 1, 2$ for the avoidance of the sth boundary of the workspace by the flock of 1-trailer systems (see Section 4.2.3);
4. $\sigma_{imk} > 0$, $m = 1, 2$ for the collision avoidance of the 1-trailer systems with the boids (see Section 4.2.4);
5. $\beta_{muij} > 0$, $j = 1, \ldots, n$, $j \neq i$, $m = u = 1, 2$ for the collision between any two 1-trailer systems (see Section 4.2.4);
6. $\psi_k > 0$, for a cohesive swarm of boids, that is, for the strength of attraction between the kth boid and the swarm centroid (see Section 4.3.1);
7. $\eta_{ks} > 0$, $s = 1, \ldots, 4$, for the collision avoidance of the sth boundary of the workspace by the swarm of boids (see Section 4.3.2);
8. $\rho_{ka} > 0$, for the collision avoidance between any two boids in the swarm (see Section 4.3.3).
9. $\zeta_{kl} > 0$, $l = 1, \ldots, q$, for the collision avoidance of qth disk-shaped obstacles by the swarm of boids (see Section 4.3.4);

Using these *tuning parameters*, we now propose the following Lyapunov function for system (7) with two components, namely the attractive and repulsive potential field functions:

$$
\begin{aligned}
L(\mathbf{x}) := \sum_{i=1}^{n} &\left[V_i(\mathbf{x}) + G_i(\mathbf{x}) \left(\sum_{m=1}^{2} \sum_{l=1}^{q} \frac{\alpha_{iml}}{FO_{iml}(\mathbf{x})} + \sum_{s=1}^{4} \frac{\gamma_{is}}{DC_{is}(\mathbf{x})} + \sum_{m=1}^{2} \sum_{s=1}^{4} \frac{\tau_{ims}}{WT_{ims}(\mathbf{x})} \right. \right. \\
&\left. + \sum_{k=1}^{h} \sum_{m=1}^{2} \frac{\sigma_{imk}}{ST_{imk}(\mathbf{x})} + \sum_{\substack{j=1 \\ j \neq i}}^{n} \sum_{m=1}^{2} \sum_{u=1}^{2} \frac{\beta_{muij}}{MT_{muij}(\mathbf{x})} \right) \Bigg] \\
&+ \sum_{i=1}^{n} \sum_{k=1}^{h} G_i(\mathbf{x}) \left[\psi_k R_k(\mathbf{x}) + R_k(\mathbf{x}) \left(\sum_{s=1}^{4} \frac{\eta_{ks}}{WB_{ks}(\mathbf{x})} + \sum_{\substack{a=1 \\ a \neq k}}^{h} \frac{\rho_{ka}}{SB_{ka}(\mathbf{x})} \right. \right. \\
&\left. \left. + \sum_{l=1}^{q} \frac{\zeta_{kl}}{FB_{kl}(\mathbf{x})} \right) \right].
\end{aligned}
\tag{20}
$$

5.2. Nonlinear acceleration-based controllers

The feedback control laws for the kinodynamic system are extracted by finding the time derivative of the various components of $L(\mathbf{x})$ along a solution of the dynamic system Eq. (7) and force $L(\mathbf{x})$ to be at least semi-negative definite. The principal goal is to establish a prescribed formation, facilitate split/rejoin maneuvers of the 1-trailer systems within a constrained and dynamic environment, and reach the target configuration with the original formation. The subtasks include restrictions placed on the workspace, convergence to predefined target, collision avoidance with fixed and moving obstacles, collision avoidance with the swarm of boids and consideration of kinodynamic constraints. Utilizing the attractive and repulsive potential field functions and upon suppressing $\mathbf{x}$, the following continuous time-invariant acceleration and velocity control laws can be generated for $\mathcal{A}_i$ and $\mathcal{B}_k$, respectively:

$$
\left.
\begin{aligned}
\sigma_{i1} &:= -\left[\delta_{i1} v_i + (f_{i1} + f_{i3}) \cos \theta_{i1} + (f_{i2} + f_{i4}) \sin \theta_{i1} \right] / g_{i3}, \\
\sigma_{i2} &:= -\left[\delta_{i2} \omega_{i1} + \tfrac{L_{i1}}{2} (f_{i2} \cos \theta_{i1} - f_{i1} \sin \theta_{i1}) + g_{i1} \right] / g_{i4}, \\
\sigma_{i3} &:= -\left[\delta_{i3} \omega_{i2} + \tfrac{L_{i2}+2d}{2} (f_{i3} \sin \theta_{i2} - f_{i4} \cos \theta_{i2}) + g_{i2} \right] / g_{i5}, \\
vb_k &:= -\psi_{k1} Lx_k, \qquad \omega b_k := -\psi_{k2} Ly_k,
\end{aligned}
\right\}
\tag{21}
$$

for $i = 1, \ldots, n$ and $k = 1, \ldots, h$, where $\delta_{i1}, \delta_{i2}, \delta_{i3}, \psi_{k1}, \psi_{k2} > 0$ are constants known as convergence parameters and the components of the controllers are of the form:

$$
\begin{aligned}
f_{11} := & \left(
\begin{aligned}
& 1 + \sum_{l=1}^{q} \frac{\alpha_{11l}}{FO_{11l}} + \sum_{s=1}^{4} \frac{\gamma_{1s}}{DC_{1s}} + \sum_{s=1}^{4} \frac{\tau_{11s}}{WT_{11s}} + \sum_{k=1}^{h} \frac{\sigma_{11k}}{ST_{11k}} + \sum_{j=2}^{n} \sum_{u=1}^{2} \frac{\beta_{1u1j}}{MT_{1u1j}} \\
& + \sum_{k=1}^{h} \left[\psi_k R_k + R_k \left(\sum_{s=1}^{4} \frac{\eta_{ks}}{WB_{ks}} + \sum_{\substack{a=1 \\ a \neq k}}^{h} \frac{\rho_{ka}}{SB_{ka}} + \sum_{l=1}^{q} \frac{\zeta_{kl}}{FB_{kl}} \right) \right]
\end{aligned}
\right) (x_{11} - p_{11}) \\
& - \sum_{i=2}^{n} \left(1 + \sum_{l=1}^{q} \frac{\alpha_{i1l}}{FO_{i1l}} + \sum_{s=1}^{4} \frac{\gamma_{is}}{DC_{is}} + \sum_{s=1}^{4} \frac{\tau_{i1s}}{WT_{i1s}} + \sum_{k=1}^{h} \frac{\sigma_{i1k}}{ST_{i1k}} + \sum_{\substack{j=1 \\ i \neq j}}^{n} \sum_{u=1}^{2} \frac{\beta_{1u1j}}{MT_{1u1j}} \right) (x_{i1} - p_{i1}) \\
& - G_1 \left(
\begin{aligned}
& \sum_{l=1}^{q} \frac{\alpha_{11l}}{FO_{11l}^2} (x_{11} - o_{l1}) + \left(\frac{\tau_{113}}{WT_{113}^2} - \frac{\tau_{111}}{WT_{111}^2} \right) + \sum_{k=1}^{h} \frac{\sigma_{11k}}{ST_{11k}^2} (x_{11} - xb_k) \\
& + \sum_{j=2}^{n} \sum_{u=1}^{2} \frac{\beta_{1u1j}}{MT_{1u1j}^2} (x_{11} - x_{ju})
\end{aligned}
\right),
\end{aligned}
$$

$$
\begin{aligned}
f_{12} := & \left(
\begin{aligned}
& 1 + \sum_{l=1}^{q} \frac{\alpha_{11l}}{FO_{11l}} + \sum_{s=1}^{4} \frac{\gamma_{1s}}{DC_{1s}} + \sum_{s=1}^{4} \frac{\tau_{11s}}{WT_{11s}} + \sum_{k=1}^{h} \frac{\sigma_{11k}}{ST_{11k}} + \sum_{j=2}^{n} \sum_{u=1}^{2} \frac{\beta_{1u1j}}{MT_{1u1j}} \\
& + \sum_{k=1}^{h} \left[\psi_k R_k + R_k \left(\sum_{s=1}^{4} \frac{\eta_{ks}}{WB_{ks}} + \sum_{\substack{a=1 \\ a \neq k}}^{h} \frac{\rho_{ka}}{SB_{ka}} + \sum_{l=1}^{q} \frac{\zeta_{kl}}{FB_{kl}} \right) \right]
\end{aligned}
\right) (y_{11} - p_{12}) \\
& - \sum_{i=2}^{n} \left(1 + \sum_{l=1}^{q} \frac{\alpha_{i1l}}{FO_{i1l}} + \sum_{s=1}^{4} \frac{\gamma_{is}}{DC_{is}} + \sum_{s=1}^{4} \frac{\tau_{i1s}}{WT_{i1s}} + \sum_{k=1}^{h} \frac{\sigma_{i1k}}{ST_{i1k}} + \sum_{\substack{j=1 \\ i \neq j}}^{n} \sum_{u=1}^{2} \frac{\beta_{1u1j}}{MT_{1u1j}} \right) (y_{i1} - p_{i2}) \\
& - G_1 \left(
\begin{aligned}
& \sum_{l=1}^{q} \frac{\alpha_{11l}}{FO_{11l}^2} (y_{11} - o_{l2}) + \frac{\tau_{112}}{WT_{112}^2} - \frac{\tau_{114}}{WT_{114}^2} + \sum_{k=1}^{h} \frac{\sigma_{11k}}{ST_{11k}^2} (y_{11} - xb_k) \\
& + \sum_{j=2}^{n} \sum_{u=1}^{2} \frac{\beta_{1u1j}}{MT_{1u1j}^2} (y_{11} - y_{ju})
\end{aligned}
\right),
\end{aligned}
$$

and for $i = 2, \ldots, n$,

$$
\begin{aligned}
f_{i1} := & \left(
\begin{aligned}
& 1 + \sum_{l=1}^{q} \frac{\alpha_{i1l}}{FO_{i1l}} + \sum_{s=1}^{4} \frac{\gamma_{is}}{DC_{is}} + \sum_{s=1}^{4} \frac{\tau_{i1s}}{WT_{i1s}} + \sum_{k=1}^{h} \frac{\sigma_{i1k}}{ST_{i1k}} + \sum_{\substack{j=1 \\ j \neq i}}^{n} \sum_{u=1}^{2} \frac{\beta_{1uij}}{MT_{1uij}} \\
& + \sum_{k=1}^{h} \left[\psi_k R_k + R_k \left(\sum_{s=1}^{4} \frac{\eta_{ks}}{WB_{ks}} + \sum_{\substack{a=1 \\ a \neq k}}^{h} \frac{\rho_{ka}}{SB_{ka}} + \sum_{l=1}^{q} \frac{\zeta_{kl}}{FB_{kl}} \right) \right]
\end{aligned}
\right) (x_{i1} - p_{i1}) \\
& - G_i \left(\sum_{l=1}^{q} \frac{\alpha_{i1l}}{FO_{i1l}^2} (x_{i1} - o_{l1}) \right) - G_i \left(\left(\frac{\tau_{i13}}{WT_{i13}^2} - \frac{\tau_{i11}}{WT_{i11}^2} \right) + \sum_{k=1}^{h} \frac{\sigma_{i1k}}{ST_{i1k}^2} (x_{i1} - xb_k) \right) \\
& + \sum_{\substack{j=1 \\ j \neq i}}^{n} \sum_{u=1}^{2} \left(G_j \frac{\beta_{u1ji}}{MT_{u1ji}^2} (x_{ju} - x_{i1}) - G_i \frac{\beta_{1uij}}{MT_{1uij}^2} (x_{i1} - x_{ju}) \right),
\end{aligned}
$$

$$f_{i2} := \left(\begin{matrix} 1 + \sum_{l=1}^{q} \frac{\alpha_{i1l}}{FO_{i1l}} + \sum_{s=1}^{4} \frac{\gamma_{is}}{DC_{is}} + \sum_{s=1}^{4} \frac{\tau_{i1s}}{WT_{i1s}} + \sum_{k=1}^{h} \frac{\sigma_{i1k}}{ST_{i1k}} + \sum_{\substack{j=1 \\ j \neq i}}^{n} \sum_{u=1}^{2} \frac{\beta_{1uij}}{MT_{1uij}} \\ + \sum_{k=1}^{h} \left[\psi_k R_k + R_k \left(\sum_{s=1}^{4} \frac{\eta_{ks}}{WB_{ks}} + \sum_{\substack{a=1 \\ a \neq k}}^{h} \frac{\rho_{ka}}{SB_{ka}} + \sum_{l=1}^{q} \frac{\zeta_{kl}}{FB_{kl}} \right) \right] \end{matrix} \right) (y_{i1} - p_{i2})$$

$$- G_i \left(\sum_{l=1}^{q} \frac{\alpha_{i1l}}{FO_{i1l}^2} (y_{i1} - o_{l2}) \right) - G_i \left(\left(\frac{\tau_{i12}}{WT_{i12}^2} - \frac{\tau_{i14}}{WT_{i14}^2} \right) + \sum_{k=1}^{h} \frac{\sigma_{i1k}}{ST_{i1k}^2} (y_{i1} - xb_k) \right)$$

$$+ \sum_{\substack{j=1 \\ j \neq i}}^{n} \sum_{u=1}^{2} \left(G_j \frac{\beta_{u1ji}}{MT_{u1ji}^2} (y_{ju} - y_{i1}) - G_i \frac{\beta_{1uij}}{MT_{1uij}^2} (y_{i1} - y_{ju}) \right).$$

Moreover, for $i = 1, \ldots, n$

$$f_{i3} := -G_i \left(\sum_{l=1}^{q} \frac{\alpha_{i2l}}{FO_{i2l}^2} (x_{i2} - o_{l1}) + \left(\frac{\tau_{i23}}{WT_{i23}^2} - \frac{\tau_{i21}}{WT_{i21}^2} \right) + \sum_{k=1}^{h} \frac{\sigma_{i2k}}{ST_{i2k}^2} (x_{i2} - xb_k) \right)$$

$$+ \sum_{\substack{j=1 \\ j \neq i}}^{n} \sum_{u=1}^{2} \left(G_j \frac{\beta_{u2ji}}{MT_{u2ji}^2} (x_{ju} - x_{i2}) - G_i \frac{\beta_{2uij}}{MT_{2uij}^2} (x_{i2} - x_{ju}) \right),$$

$$f_{i4} := -G_i \left(\sum_{l=1}^{q} \frac{\alpha_{i2l}}{FO_{i2l}^2} (y_{i2} - o_{l2}) + \left(\frac{\tau_{i22}}{WT_{i22}^2} - \frac{\tau_{i24}}{WT_{i24}^2} \right) + \sum_{k=1}^{h} \frac{\sigma_{i2k}}{ST_{i2k}^2} (y_{i2} - xb_k) \right)$$

$$+ \sum_{\substack{j=1 \\ j \neq i}}^{n} \sum_{u=1}^{2} \left(G_j \frac{\beta_{u2ji}}{MT_{u2ji}^2} (y_{ju} - y_{i2}) - G_i \frac{\beta_{2uij}}{MT_{2uij}^2} (y_{i2} - y_{ju}) \right),$$

$$g_{i1} := -G_i \frac{\gamma_{i4}}{DC_{i4}^2} (\theta_{i2} - \theta_{i1}), \quad g_{i2} := G_i \frac{\gamma_{i4}}{DC_{i4}^2} (\theta_{i2} - \theta_{i1}), \quad g_{i3} := 1 + G_i \frac{\gamma_{i1}}{DC_{i1}^2},$$

$$g_{i4} := 1 + G_i \frac{\gamma_{i2}}{DC_{i2}^2}, \quad g_{i5} := 1 + G_i \frac{\gamma_{i3}}{DC_{i3}^2},$$

$$Lx_k := G_i \left(\psi_k + \sum_{s=1}^{4} \frac{\eta_{ks}}{WB_{ks}} + \sum_{\substack{a=1 \\ a \neq k}}^{h} \frac{\rho_{ka}}{SB_{ka}} + \sum_{l=1}^{q} \frac{\zeta_{kl}}{FB_{kl}} \right) \left(xb_k - \frac{1}{h} \sum_{a=1}^{h} xb_a \right)$$

$$+ R_k G_i \left(\frac{\eta_{k3}}{WB_{k3}^2} - \frac{\eta_{k1}}{WB_{k1}^2} \right) - 2 R_k G_i \sum_{\substack{a=1 \\ a \neq k}}^{h} \frac{\rho_{ka}}{SB_{ka}^2} (xb_k - xb_a) - R_k G_i \sum_{l=1}^{q} \frac{\zeta_{kl}}{FB_{kl}} (xb_k - o_{l1}),$$

$$Ly_k := G_i \left(\psi_k + \sum_{s=1}^{4} \frac{\eta_{ks}}{WB_{ks}} + \sum_{\substack{a=1 \\ a \neq k}}^{h} \frac{\rho_{ka}}{SB_{ka}} + \sum_{l=1}^{q} \frac{\zeta_{kl}}{FB_{kl}} \right) \left(yb_k - \frac{1}{h} \sum_{a=1}^{h} yb_a \right)$$

$$+ R_k G_i \left(\frac{\eta_{k2}}{WB_{k2}^2} - \frac{\eta_{k4}}{WB_{k4}^2} \right) - 2 R_k G_i \sum_{\substack{a=1 \\ a \neq k}}^{h} \frac{\rho_{ka}}{SB_{ka}^2} (yb_k - yb_a) - R_k G_i \sum_{l=1}^{q} \frac{\zeta_{kl}}{FB_{kl}} (yb_k - o_{l2}).$$

Algorithm 1 Pseudocode for the numerical solution of the LbCS

Require: Time for executing the simulation, $T_{\max}$
    for $t = 1 : T_{\max}$ **do**
Require: Numerical values of initial state, constraints, and control and convergence parameters.
      for $i = 1 : n$ **do**
        Evaluate all the attractive and repulsive potential field functions for the 1-trailer systems, and its associated control laws.
      end for
      for $k = 1 : h$ **do**
        Evaluate all the attractive and repulsive potential field functions for the swarm of boids, and its associated control laws.
      end for
Require: The combined dynamic model of the steerable 1-trailer system and the swarm of boids, Eq. (7) for the ODE Solver in Mathematica.
      for $i = 1 : n$ **do**
        Evaluate the equations of motion for the 1-trailer system sing the Mathematica ODE Solver.
      end for
      for $k = 1 : h$ **do**
        Evaluate equations of motion for the swarm of boids sing the Mathematica ODE Solver.
      end for
Require: Animate the output from the ODE Solver.
    end for

---

6. Stability Analysis

In this section, we will analyze the stability of system (7).

Theorem 1. *If a fixed point* $\mathbf{x}_i^* = (p_{i1}, p_{i2}, p_{i3}, p_{i4}, 0, 0, 0) \in \mathbb{R}^7$ *is an equilibrium point of* $\mathcal{A}_i$, $i = 1, \ldots, n$, *then* $\mathbf{x}^* = (\mathbf{x}_1^*, \mathbf{x}_2^*, \ldots, \mathbf{x}_n^*) \in D(L(\mathbf{x}))$ *is a stable equilibrium point of system* (7).

Proof. One can easily verify the following, for $i \in \{1, \ldots, n\}$ and $k \in \{1, \ldots, h\}$:

1. $L(\mathbf{x})$ is defined, continuous, and positive over the domain $D(L(\mathbf{x})) = \{\mathbf{x} \in \mathbb{R}^{7n} : FO_{iml}(\mathbf{x}) > 0, l = 1, \ldots, q, m = 1, 2; DC_{is}(\mathbf{x}) > 0, s = 1, \ldots, 4; WT_{ims}(\mathbf{x}) > 0, m = 1, 2, s = 1, \ldots, 4; ST_{imk}(\mathbf{x}) > 0, m = 1, 2; MT_{muij}(\mathbf{x}) > 0, m = 1, 2, u = 1, 2, j = 1, \ldots, n, j \neq i; WB_{ks}(\mathbf{x}) > 0, s = 1, \ldots, 4; SB_{ka}(\mathbf{x}) > 0, a = 1, \ldots, h, a \neq k; FB_{kl}(\mathbf{x}) > 0, l = 1, \ldots, q\};$
2. $L(\mathbf{x}^*) = 0;$
3. $L(\mathbf{x}) > 0 \ \forall \mathbf{x} \in D(L(\mathbf{x}))/\mathbf{x}^*.$

Next, consider the time derivative of the Lyapunov function along a particular trajectory of system (7).

$$\dot{L}_{(7)}(\mathbf{x}) := \sum_{i=1}^{n} \left[f_{i1}\dot{x}_{i1} + f_{i2}\dot{y}_{i1} + f_{i3}\dot{x}_{i2} + f_{i4}\dot{y}_{i2} + \sum_{m=1}^{2} \left(g_{im}\dot{\theta}_{im} + g_{i\,m+3}\omega_{im}\dot{\omega}_{im} \right) + g_{i3}v_i\dot{v}_i \right]$$
$$+ \sum_{k=1}^{h} \left[Lx_k\dot{x}b_k + Ly_k\dot{y}b_k \right].$$

Substituting the controllers given in Eq. (21) and the governing ODEs for system (7), we obtain the following semi-negative definite function:

$$\dot{L}_{(7)}(\mathbf{x}) := - \left[\sum_{i=1}^{n} \left(\delta_{i1}v_i^2 + \delta_{i2}\omega_{i1}^2 + \delta_{i3}\omega_{i2}^2 \right) + \sum_{k=1}^{h} \left(\psi_{k1}Lx_k^2 + \psi_{k2}Ly_k^2 \right) \right] \leq 0.$$
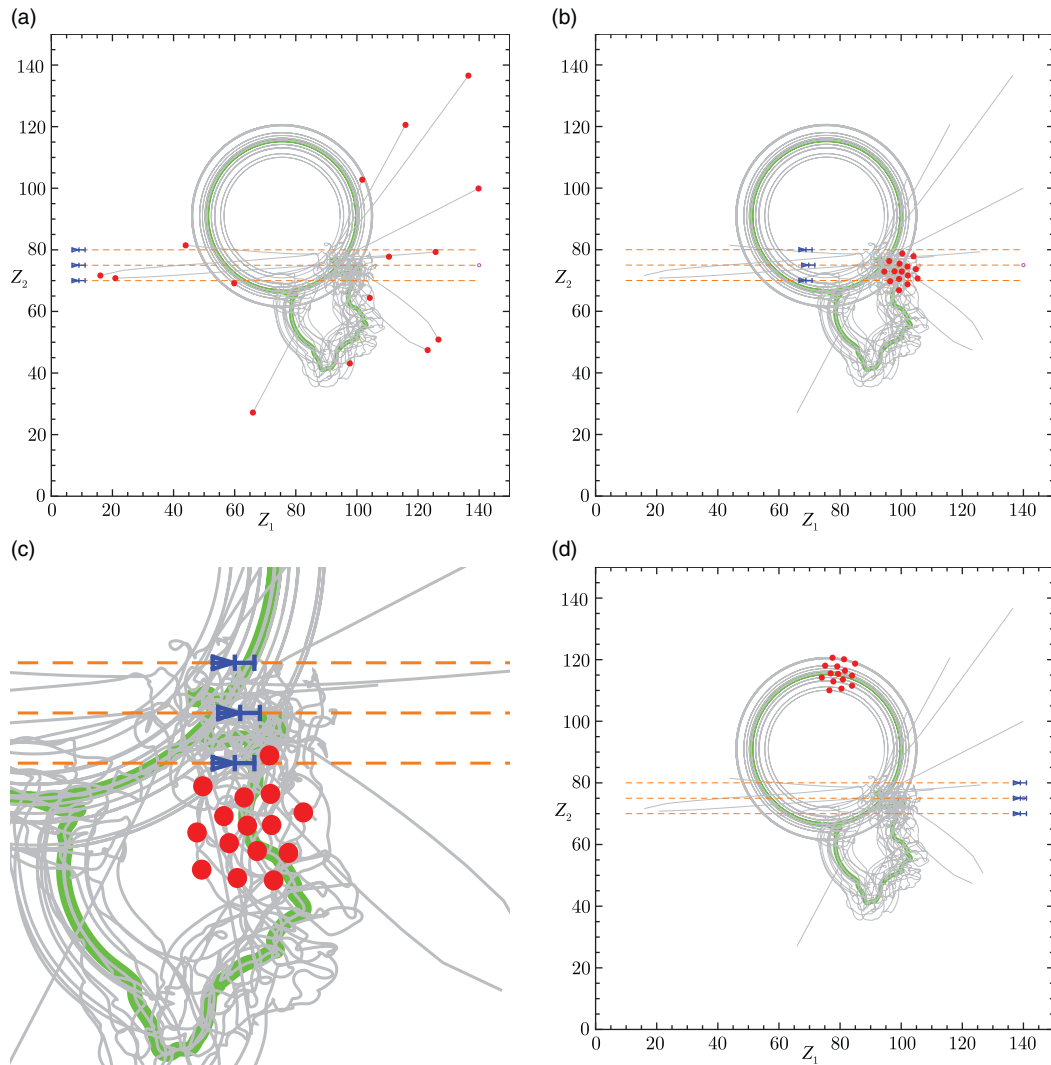
Fig. 6. Scenario 1 showing the evolution of trajectories of the 1-trailer robots and the emergent behavior of the swarm, $h = 15$ boids (shown in red), randomly positioned at the initial time $t = 0$. The gray lines show the trajectories of the individuals in the swarm. The 1-trailer robots are shown in blue with the orange line as its trajectory. The path of the swarm centroid shown in green. The 1-trailer systems are shown in blue with its trajectories in orange. (a) The initial positions of the 1-trailer robots and the swarm of boids at $t = 0$ units. (b) The avoidance between the 1-trailer robots and the swarm of boids at $t = 9500$ units. (c) The avoidance between the 1-trailer robots and the swarm of boids at $t = 30, 100$ units. (d) The final postures of the 1-trailer robots and the position of the swarm at $t = 50, 000$ units.

Thus, $\dot{L}_{(7)}(\mathbf{x}) \, \forall \mathbf{x} \in D(L(\mathbf{x}))$ and $\dot{L}_{(7)}(\mathbf{x}^*) = 0$. Finally, it can be easily verified that $L(\mathbf{x}) \in C^1(D(L(\mathbf{x})))$, which makes up the fifth and final criterion of a Lyapunov function. Hence, $\mathbf{x}^*$ is a stable equilibrium point in the sense of Lyapunov. □

7. Simulation Results

This section demonstrates the effectiveness of the proposed continuous time-invariant nonlinear control laws within the framework of the LbCS via computer simulations of virtual scenarios where a flock of 1-trailer robots navigates to a final configuration while avoiding fixed and moving obstacles en route target. The fixed obstacles are the disk-shaped obstacles while the moving obstacles for the 1-trailer robots are the other 1-trailer robots and the swarm of boids. Upon encountering an obstacle, the articulated 1-trailer system in formation splits and circumnavigates the obstacle. The robots then rejoin into their coherent group and the formation is re-established before reaching the final target configuration. The stability results are verified numerically.

Table I. Scenario 1. Numerical values of initial state, constraints, and control and convergence parameters.

Initial states of the 1-trailer robots	
Rectangular position	$(x_{11}, y_{11}) = (10, 75)$, $(x_{21}, y_{21}) = (10, 80)$, and $(x_{31}, y_{31}) = (10, 70)$
Angular positions	$\theta_{i1} = \theta_{i2} = 0$, for $i = 1, \ldots, 3$
Translational velocities	$v_1 = 0.5, v_2 = v_3 = 3$
Rotational velocities	$\omega_{i1} = \omega_{i2} = \pi/360$ for $i = 1, \ldots, 3$
Constraints	
Dimension of robot	$L_{i1} = 2$, $L_{i2} = 1.2$ and $l_i = 0.5$, for $i = 1, \ldots, 3$
Leader rarget	$(p_{11}, p_{12}) = (140, 75)$
Position of ghost targets	$(a_2, b_2) = (0, -5)$ and $(a_3, b_3) = (0, 5)$
Max. translational velocity	$v_{max} = 10$
Max. steering angle	$\phi_{max} = \pi/2$
Max. rot. velocity of trailer	$\omega_{2\,max} = 1$
Min. turning radius	$\rho_{min} = 0.75$
Clearance parameters	$\epsilon_1 = 0.1$ and $\epsilon_2 = 0.2$
Workspace boundaries	$\eta_1 = \eta_2 = 150$
Parameters for the 1-trailer robots	
Dynamic constraints	$\gamma_{is} = 0.1$, for $i = 1, \ldots, 3$ and $s = 1, \ldots, 4$
Boundary limitations	$\tau_{ims} = 0.0001$, for $i = 1, \ldots, 3$, $m = 1, 2$ and $s = 1, \ldots, 4$
Avoidance of boids	$\kappa_{imk} = 1$, for $i = 1, \ldots, 3$, $m = 1, 2$ and $k = 1, \ldots, 15$
Inter-robot collision avoidance	$\beta_{muij} = 0.01$, for $m = u = 1, 2$ and $i, j = 1, \ldots, 3$, $i \neq j$
Convergence	$\delta_{i1} = \delta_{i2} = \delta_{i3} = 5000$, for $i = 1, \ldots, 3$
Parameters for the boids	
Bin size	1
Cohesion parameter	$\psi_k = 25$, for $k = 1, \ldots, 15$
Boundary limitations	$\eta_{ks} = 0.0001$, for $k = 1, \ldots, 15$ and $s = 1, \ldots, 4$
Inter-boid avoidance	$\rho_{ka} = \text{rand}[100, 500]$, for $a, k = 1, \ldots, 15$, $a \neq k$
Convergence	$\alpha_{k1} = \alpha_{k2} = 0.01$, for $k = 1, \ldots, 15$

The pseudocode for the implementation of the LbCS for dynamic model, Eq. (7) is in Algorithm 1.

7.1. Scenario 1

There are 3 1-trailer robots and their initial positions are chosen while we utilize the randomization technique to place the 15 boids of the swarm within the workspace, as shown in Fig. 6. The flock of 1-trailer system navigate to a final configuration while avoiding each other, the fixed and moving obstacles en route their target using V2V and V2I communications. For the swarm of boids, first, the boids converge to the swarm centroid, move randomly and then form an emergent circular behavior. A general split–rejoin and avoidance behavior is observed of the 1-trailer system. This could be mimicking a herd of cows crossing an intersection. In this scenario, we take $\alpha_{iml} = \zeta_{kl} = 0$, assuming that there are no fixed obstacles in the workspace. Table I provides all the values of the initial conditions, constraints,s and different parameters utilized in the simulation. Figure 6(a) shows the initial positions of the 1-trailer systems and the boids. Figure 6(b) illustrates the avoidance and motion of the flock of 1-trailer systems and swarm of boids. Figure 6(c) is a zoomed-in illustration of the proximity of the 1-trailer systems to the swarm of boids. The control parameters are chosen such that a safe-zoning in avoidance is achieved. Figure 6(d) shows the final configuration of the 1-trailer systems and the swarm of boids.

Table II. Scenario 2. Numerical values of initial state, constraints, and control and convergence parameters.

Initial states of the 1-trailer robots	
Rectangular position	$(x_{11}, y_{11}) = (10, 54)$ and $(x_{21}, y_{21}) = (10, 77)$
Angular positions	$\theta_{i1} = \theta_{i2} = 0$, for $i = 1, 2$
Translational velocities	$v_1 = 1$ and $v_2 = 3$
Rotational velocities	$\omega_{i1} = \omega_{i2} = \pi/360$, for $i = 1, 2$
Constraints	
Dimension of robot	$L_{i1} = 2$, $L_{i2} = 1.2$ and $l_i = 0.5$, for $i = 1, 2$
Leader target	$(p_{11}, p_{12}) = (80, 55)$
Position of ghost targets	$(a_2, b_2) = (0, -5)$
Workspace boundaries	$\eta_1 = \eta_2 = 100$
Parameters for the 1-trailer robots	
Dynamic constraints	$\gamma_{is} = 0.1$, for $i = 1, 2$ and $s = 1, \ldots, 4$
Boundary limitations	$\tau_{ims} = 0.0001$, for $i = 1, 2$, $m = 1, 2$ and $s = 1, \ldots, 4$
Avoidance of fixed obstacles	$\alpha_{iml} = 1$, for $i = 1, 2$, $m = 1, 2$ and $l = 1, \ldots, 4$
Avoidance of boids	$\kappa_{imk} = 0.01$, for $i = 1, 2$, $m = 1, 2$ and $k = 1, \ldots, 10$
Inter-robot collision avoidance	$\beta_{muij} = 0.1$, for $m = u = 1, 2$ and $i, j = 1, 2$, $i \neq j$
Convergence	$\delta_{i1} = \delta_{i2} = \delta_{i3} = 1000$, for $i = 1, 2$
Parameters for the boids	
Cohesion parameter	$\psi_k = 25$, for $k = 1, \ldots, 10$
Boundary limitations	$\eta_{ks} = 0.001$, for $k = 1, \ldots, 10$ and $s = 1, \ldots, 4$
Avoidance of fixed obstacles	$\zeta_{kl} = \text{rand}[1, 5]$, for $k = 1, \ldots, 10$ and $l = 1, \ldots, 4$
Inter-boid avoidance	$\rho_{ka} = \text{rand}[100, 300]$, for $a, k = 1, \ldots, 10$, $a \neq k$
Convergence	$\alpha_{k1} = \alpha_{k2} = 0.05$, for $k = 1, \ldots, 10$

It is interesting to see that our artificial swarm mimics nature. The biological swarm behavior is a natural phenomenon which can be used to develop a nature-inspired algorithm. As humans, we observe the natural phenomenon and then create and test a model that mimics the natural phenomenon. After various testing of the model via simulations and further refinement, the refined model can be used to extract a metaheuristic as a basis to finally design and tune a nature-inspired algorithm.

7.2. Scenario 2

The scenario in Fig. 7 considers 2 1-trailer robots and 10 boids in the swarm. The 1-trailer robots move to their final destination while avoiding each other, the swarm of boids and the disk-shaped fixed obstacles using V2V and V2I communications. This scenario could be mimicking a traffic-like situation whereby the autonomous vehicles have to avoid heavy traffic such as of those containing multiple heterogeneous system. The emergent leader–follower behavior of the swarm of boids depicts a virtual scenario whereby a flock of birds move about in a workspace cluttered with obstacles. For the swarm of boids with an emergent leader–follower-like behavior, we expect an individual with a low cohesion parameter to be further away from a more compactly arranged group of individuals with more or less the same, but higher, cohesion parameters. Because of the effects of the attraction and the inter-individual collision avoidance functions in the Lyapunov function, the individual with the lower cohesion parameter can either be following or leading the group. The corresponding initial and final states, and other essential data are provided in Table II, if the values therein are different from those in the previous scenario shown in Table I. Figure 7(a) shows the initial positions of the 2 1-trailer systems and the 10 boids. Figure 7(b) and (c) are zoomed-in snapshots showing the proximity of the tractor–trailer pair of robots to the swarm. Figure 7(d) shows the final configuration of the 1-trailer systems and the swarm of boids.
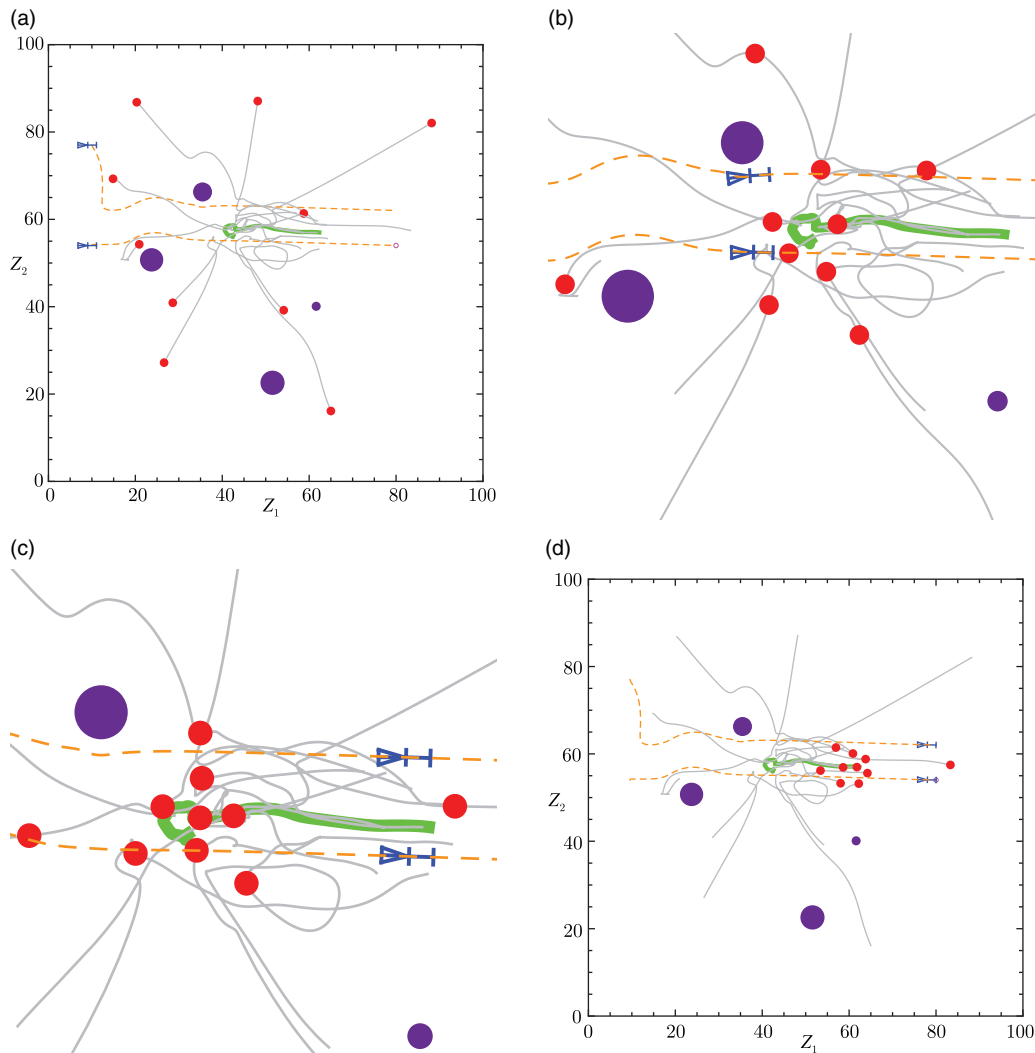
Fig. 7. Scenario 2 showing the trajectories of the 1-trailer robots and the swarm of boids at different times of the journey, including the obstacle and collision avoidance. The $h = 10$ boids (shown in red) are randomly positioned at the initial time $t = 0$. The gray lines show the trajectories of the individuals of the swarm with the swarm centroid in green. The 1-trailer robots are shown in blue with its trajectories in orange. The disk-shaped fixed obstacles are shown in purple. (a) The initial positions of the 1-trailer robots and the swarm of boids at $t = 0$ units. (b) The avoidance between the 1-trailer robots and the swarm of boids at $t = 10, 000$ units. (c) The avoidance between the 1-trailer robots and the swarm of boids at $t = 30, 400$ units. (d) The final postures of the 1-trailer robots and the position of the swarm at $t = 50, 000$ units.

7.3. Scenario 3

The nonlinear controllers for system (7), σ_{i1}, σ_{i2}, σ_{i3}, vb_k and ωb_k, for $i = 1, 2$ and $k = 1, \ldots, 10$ were simulated to generate feasible vehicle trajectories, as illustrated in Figure 8. Noting that the number of boids is 10 and the number of 1-trailer robots is 2 and assuming the units have been appropriately taken care of, initial conditions pertaining to the kinodynamic system (7) and other essentials of the situation are provided in Table III, if the values therein are different from those in the previous scenario shown in Table I or Table II. The 1-trailer robots are observed to move to their final configuration while avoiding each other, the swarm of boids and the disk-shaped fixed obstacles, again using V2V and V2I communications via wireless technology. The swarm of boids shows a behavior that changes from a seemingly random one, to a swirling structure and then to an oscillating one about a stationary point. In this emergent pattern, the swarm, as one cohesive group, forms a ring about the point and circulate continuously along the ring, as in a rotating school of fish.[55] The resultant emergent behavior in this virtual scenario by the communication system is a consequence of the interaction between the boids and the environment they are exposed to; therefore,
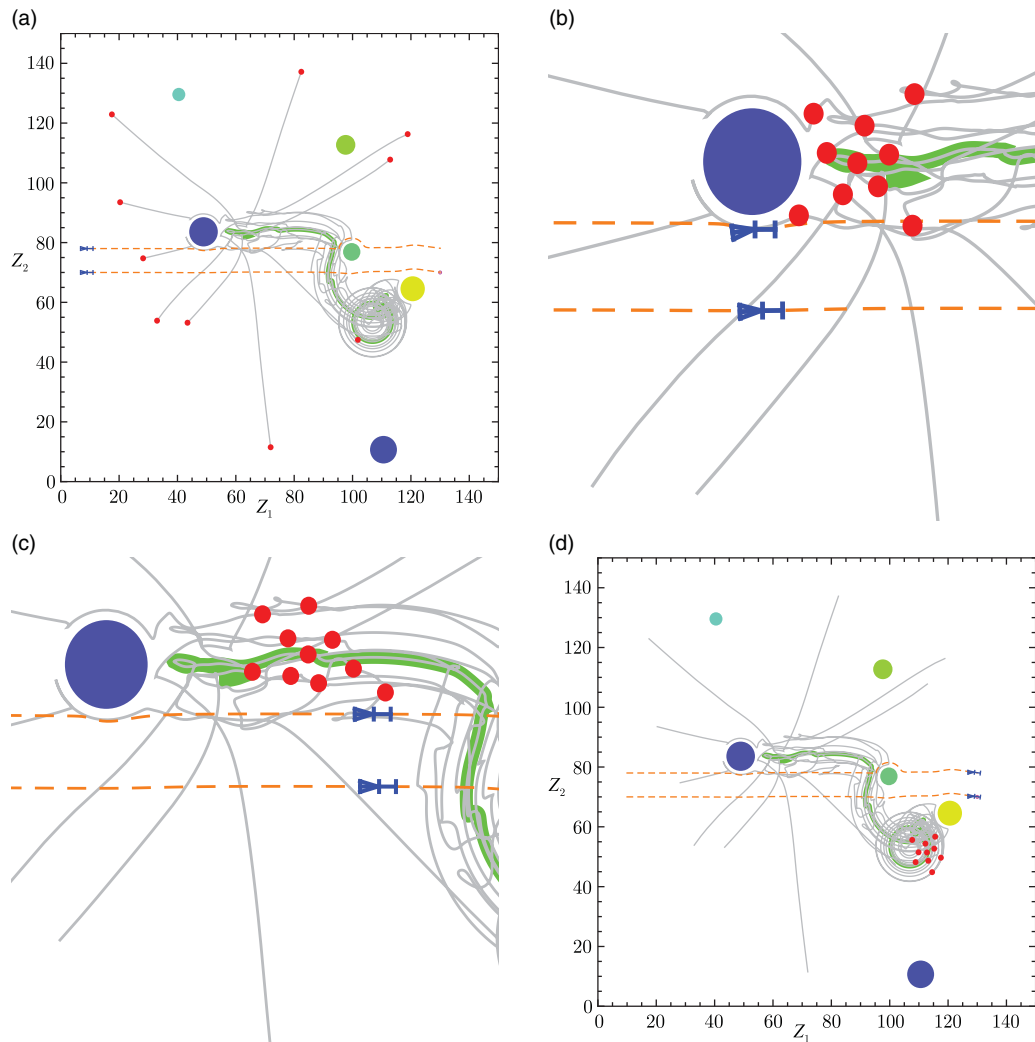
Fig. 8. Scenario 3 showing the trajectories of the 1-trailer robots and randomly positioned swarm of boids ($n = 10$, shown in red), including the obstacle and collision avoidance. The gray lines show the trajectories of the individuals of the swarm with the swarm centroid in green. The 1-trailer robots are shown in blue with its trajectories in orange. Also, there are 6 randomly placed disk-shaped obstacles shown in different colors. (a) The initial positions of the 1-trailer robots and the swarm of boids at $t = 0$ units. (b) The avoidance between the 1-trailer robots and the swarm of boids at $t = 10, 500$ units. (c) The avoidance between the 1-trailer robots and the swarm of boids at $t = 25, 700$ units. (d) The final postures of the 1-trailer robots and the position of the swarm at $t = 50, 000$ units.

it becomes difficult to predict the types of emergent behavior in general.[9] It is notable in this scenario that the swarm formation can also change to adapt to the environment.[56] Figure 7(a) shows the initial positions of the 2 1-trailer systems and the 10 boids. Figure 7(b) and (c) are zoomed-in illustrations showing the proximity of the tractor–trailer pair of robots to the swarm. Figure 7(d) shows the final configuration of the 1-trailer systems and the swarm of boids.

7.4. Scenario 4
This virtual scenario shows a split–rejoin maneuver by the flock of 1-trailer robots in the communication system. The initial positions of the 1-trailer ronots are assigned, whereas for those of the boids in the swarm are randomly generated in the workspace, as illustrated in Fig. 9. The 1-trailer robots reach their designated target while avoiding each other and the obstacles in the workspace. They also avoid the swarm of boids which is exhibiting a circular behavior. The corresponding initial and final states, and other essential data are provided in Table IV, if the values therein are different from those in Scenario 1 as shown in Table I.

Table III. Scenario 3. Numerical values of initial state, constraints, and control and convergence parameters. There are 2 1-trailer systems and 10 boids.

Initial states of the 1-trailer robots	
Rectangular position	$(x_{11}, y_{11}) = (10, 70)$ and $(x_{21}, y_{21}) = (10, 78)$
Translational velocities	$v_1 = 0.7$ and $v_2 = 0.5$

Constraints	
Leader target	$(p_{11}, p_{12}) = (130, 70)$
Workspace boundaries	$\eta_1 = \eta_2 = 150$

Parameters for the 1-trailer robots	
Avoidance of fixed obstacles	$\alpha_{iml} = 0.1$, for $i = 1, 2$, $m = 1, 2$ and $l = 1, \ldots, 6$
Avoidance of boids	$\kappa_{imk} = 0.05$, for $i = 1, 2$, $m = 1, 2$ and $k = 1, \ldots, 10$
Convergence	$\delta_{i1} = \delta_{i2} = \delta_{i3} = 5000$, for $i = 1, 2$

Parameters for the boids	
Cohesion parameter	$\psi_k = \text{rand}[10, 20]$, for $k = 1, \ldots, 10$
Avoidance of fixed obstacles	$\zeta_{kl} = 50$, for $k = 1, \ldots, 10$ and $l = 1, \ldots, 6$
Inter-boid avoidance	$\rho_{ka} = \text{rand}[5, 50]$, for $a, k = 1, \ldots, 10$, $a \neq k$

Table IV. Scenario 4. Numerical values of initial state, constraints, and control and convergence parameters.

Initial states of the 1-trailer robots	
Translational velocities	$v_1 = 0.7$, $v_2 = v_3 = 3.5$

Constraints	
Max. steering angle	$\phi_{\max} = 7\pi/18$

Parameters for the 1-trailer robots	
Avoidance of fixed obstacles	$\alpha_{iml} = 10$, for $i = 1, \ldots, 3$, $m = 1, 2$ and $l = 1, \ldots, 5$
Inter-robot collision avoidance	$\beta_{muij} = 0.01$, for $m = u = 1, 2$ and $i, j = 1, \ldots, 3$, $i \neq j$

Parameters for the boids	
Cohesion parameter	$\psi_k = 20$, for $k = 1, \ldots, 10$
Inter-boid avoidance	$\rho_{ka} = \text{rand}[50, 500]$, for $a, k = 1, \ldots, 10$, $a \neq k$
Avoidance of fixed obstacles	$\zeta_{kl} = 10$, for $k = 1, \ldots, 10$ and $l = 1, \ldots, 5$
Convergence	$\alpha_{k1} = \alpha_{k2} = 0.001$, for $k = 1, \ldots, 10$

Figure 10 shows the evolution of the Lyapunov function and its time derivative along the system trajectories for Scenario 4. It shows the periods when system (21) increases or decreases its rate of energy dissipation. The continuous evolution of the Lyapunov function also shows that the trajectories are collision-free. We restrict to providing the evolution of the Lyapunov function and its time derivative along the system trajectories for Scenario 4 only as the trend of evolution is similar for the other scenarios.

8. Conclusion
The design of multitasking problem of multi-vehicular robotic systems is a complex, computationally expensive, yet an interesting problem. In this paper, we consider a heterogeneous robotic system, which operates in unison in a dynamic workspace. This robust heterogeneous system exhibits obstacle- and collision-free trajectories using virtual V2V, V2I,s and V2E communications and mimics the dynamics of intelligent vehicle (or transport) system. The seminal aim is to design continuous
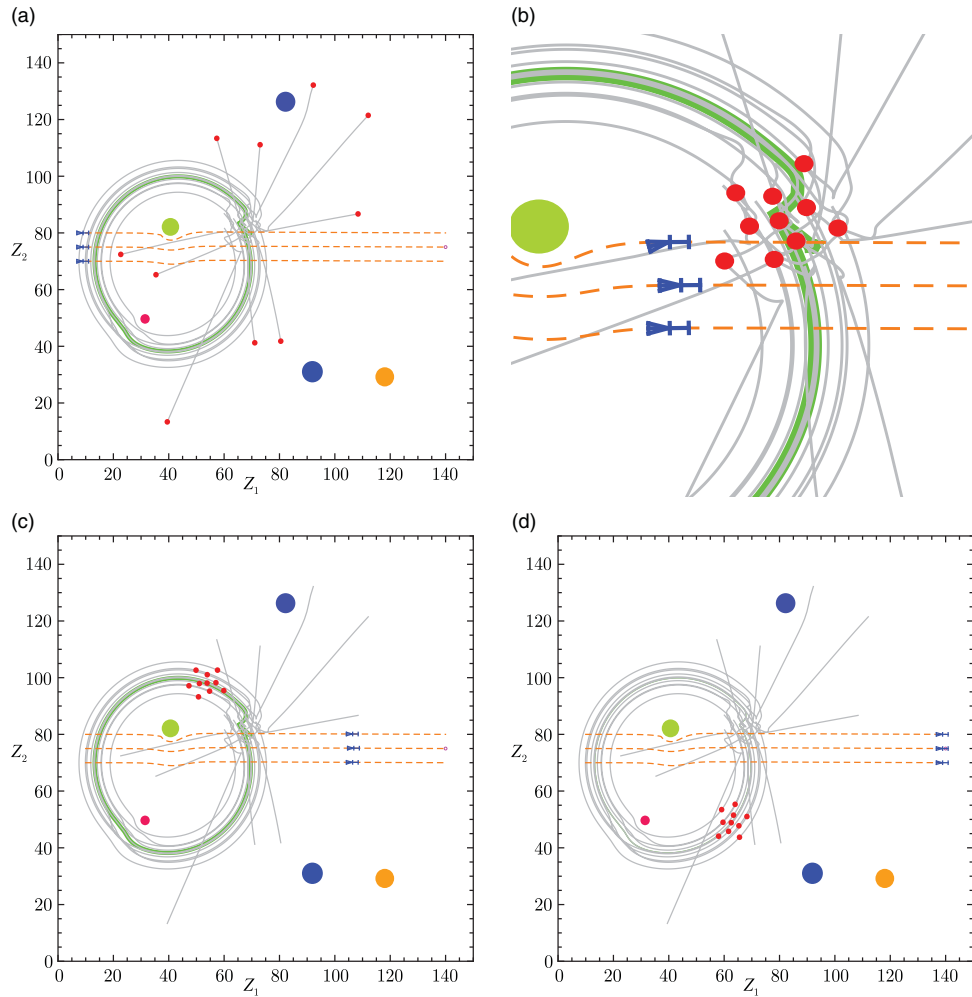
Fig. 9. Scenario 4 showing the trajectories of the 1-trailer robots and $h = 10$ (shown in red) randomly positioned boids in the workspace. The gray lines show the trajectories of the individuals of the swarm. The path of the swarm centroid is given by the green line. The 1-trailer robots are shown in blue with its trajectories in orange. There are *six* randomly placed disk-shaped obstacles shown in different colors. (a) The initial positions of the 1-trailer robots and the swarm of boids at $t = 0$ units. (b) The avoidance between the 1-trailer robots and the swarm of boids at $t = 12, 500$ units. (c) The avoidance between the 1-trailer robots and the swarm of boids at $t = 32, 700$ units. (d) The final postures of the 1-trailer robots and the position of the swarm at $t = 50, 000$ units.
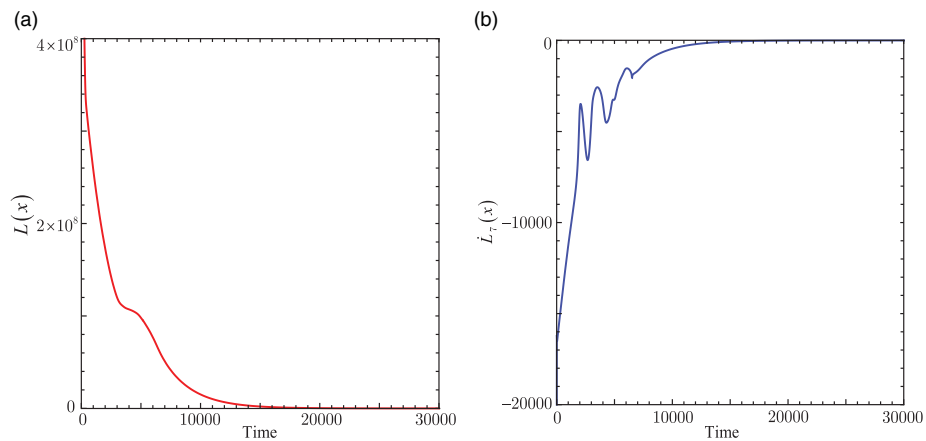

Fig. 10. Evolution of $L(\mathbf{x})$ and its time derivative $\dot{L}_{(7)}(\mathbf{x})$ for Scenario 4. (a) Behavior of the Lyapunov function, $L(\mathbf{x})$. (b) Behavior of the time derivative of the Lyapunov function, $\dot{L}_{(7)}(\mathbf{x})$.

velocity and acceleration-based time-invariant control laws using the LbCS that, *inter alia*, ensure stability of the heterogeneous system. To the authors' knowledge, this is the first time a set of stabilizing control laws have been developed for the collision avoidance of a 1-trailer system and swarm of boids within the framework of the motion planning and control problem. A big advantage of the LbCS is the simplicity in the design of the controllers and inclusion of the dynamic constraints of the heterogeneous system.

Also implementing the three flocking rules of cohesion, alignment, and separation in the differential equations governing the swarm, and varying the *tuning* parameters of the equations resulted in the emergent swarming behaviors.

The effectiveness of the proposed controllers was demonstrated by computer-based simulations that showed split and rejoin maneuvers of the flock of 1-trailer systems and emergent behaviors of the swarm.

The work presented in this paper could be used in engineering applications involving pattern formation and cooperation among the robotic systems. Future research work includes applying the LbCS motion planner to address the motion planning and control problem of a flock of quadrotors in unison with swarm of boids in *three*-dimensional space. In addition, the authors will investigate optimization methods of finding the optimized parameters.

Conflicts of Interest
The author(s) declare none.

References
1. K. Raghuwaiya, B. Sharma and J. Vanualailai, "Leader-follower based locally rigid formation control," *J. Adv. Transp.* **2018**, 14 (2018), Article ID 5278565. doi: 10.1155/2018/5278565.
2. B. Sharma, J. Vanualailai and A. Prasad, "A $d\phi$-strategy: Facilitating dual-formation control of a virtually connected team," *J. Adv. Transp.* **2017**, 17 (2017), Article ID 9213805. doi: 10.1155/2017/9213805.
3. L. Lacasa, B. Luque, F. Ballesteros, J. Luque and J. Carlos Nuño, "From time series to complex networks: The visibility graph," *Proc. National Acad. Sci.* **105**(13), 4972–4975 (2008). doi: 10.1073/pnas.0709247105.
4. R. Siegwart, I. R. Nourbakhsh and D. Scaramuzza, *Introduction to Autonomous Mobile Robots*, 2nd edn. (The MIT Press, 2011). ISBN 0262015358, 9780262015356.
5. F. Lingelbach, "Path Planning Using Probabilistic Cell Decomposition," *IEEE International Conference on Robotics and Automation*, vol. 1, New Orleans, LA (2004) pp. 467–472. doi: 10.1109/ROBOT.2004.1307193.
6. C. Niederberger, D. Radovic and M. Gross, "Generic Path Planning for Real-Time Application," *Proceedings of Computer Graphics International* (2004) pp. 299–306. doi: 10.1109/CGI.2004.1309225.
7. O. Khatib, "Real time obstacle avoidance for manipulators and mobile robots," *Int. J. Robot. Res.* **7**(1), 90–98 (1986).
8. B. Sharma, J. Vanualailai and S. Singh, "Tunnel passing maneuvers of prescribed formations," *Int. J. Robust Nonlinear Control* **24**(5), 876–901 (2014).
9. B. N. Sharma, J. Raj and J. Vanualailai, "Navigation of carlike robots in an extended dynamic environment with swarm avoidance," *Int. J. Robust Nonlinear Control* **28**(2), 678–698 (2018).
10. A. Prasad, B. Sharma, J. Vanualailai and S. A. Kumar, "A geometric approach to target convergence and obstacle avoidance of a nonstandard tractor-trailer robot," *Int. J. Robust Nonlinear Control* **30**(13), 4924–4943 (2020).
11. J. Raj, K. Raghuwaiya and J. Vanualailai, "Collision avoidance of 3D rectangular planes by multiple cooperating autonomous agents," *J. Adv. Transp.* **2020**, 13 (2020), Article ID 4723687. doi: 10.1155/2020/4723687.
12. J. Raj, K. S. Raghuwaiya and J. Vanualailai, "Novel lyapunov-based autonomous controllers for quadrotors," *IEEE Access* **8**(1), 47393–47406 (2020).
13. L. Xie, K. Stol and W. Xu, "Energy-optimal motion trajectory of an omni-directional mecanum-wheeled robot via polynomial functions," *Robotica* **38**(8), 1400–1414 (2020).
14. O. Arslan and D. E. Koditschek, "Sensor-based reactive navigation in unknown convex sphere worlds," *Int. J. Robot. Res.* **38**(2–3)196–223 (2019).
15. B. Della Corte, H. Andreasson, T. Stoyanov and G. Grisetti, "Unified motion-based calibration of mobile multi-sensor platforms with time delay estimation," *IEEE Robot. Autom. Lett.* **4**(2), 902–909 (2019).
16. Y. Zhang and K. P. Valavanis, "Sensor-based 2-d potential panel method for robot motion planning," *Robotica* **1**(1), 81–89 (1996).
17. M. Hoy, A. S. Matveev and A. V. Savkin, "Algorithms for collision-free navigation of mobile robots in complex cluttered environments: A survey," *Robotica* **33**(3), 463–497 (2015).
18. K. Shojaei, "Neural network formation control of a team of tractor-trailer systems," *Robotica* **36**(1), 39–56 (2018).

19. J. Raj, K. Raghuwaiya, J. Vanualailai and B. Sharma, "Navigation of Car-Like Robots in Three-Dimensional Space," *Proceedings of the 2018 5th Asia-Pacific World Congress on Computer Science and Engineering (APWC on CSE)* (2018) pp. 271–275.
20. B. Siciliano and O. Khatib, *Springer Handbook of Robotics*, 2nd edn. (Springer Publishing Company, Incorporated, 2016).
21. A. S. Matveev, A. V. Savkin, M. Hoy and C. Wang, "3 - Survey of Algorithms for Safe Navigation of Mobile Robots in Complex Environments," **In:** *Safe Robot Navigation Among Moving and Steady Obstacles* (A. S. Matveev, A. V. Savkin, M. Hoy and C. Wang, eds.) (Butterworth-Heinemann, 2016) pp. 21–49.
22. J.-C. Latombe, *Robot Motion Planning* (Kluwer Academic Publishers, USA, 1991).
23. D. Xu, X. Zhang, Z. Zhu, C. Chen and P. Yang, "Behavior-based formation control of swarm robots," *Math. Problems Eng.* **2014**, 13 (2014), Article ID 205759. doi: 10.1155/2014/205759.
24. K. D. Do, "Formation tracking control of unicycle-type mobile robots with limited sensing ranges," *IEEE Trans. Control Syst. Tech.* **16**(3), 527–538 (2008).
25. K. Raghuwaiya and S. Singh, "Formation types of multiple steerable 1-trailer mobile robots via split/rejoin maneuvers," *New Zealand J. Math.* **43**, 7–21 (2013).
26. B. Sharma, S. Singh, J. Vanualailai and A. Prasad, "Globally rigid formation of n-link doubly nonholonomic mobile manipulators," *Robot. Auto. Syst.* **105**, 69–84 (2018).
27. Z. Yang, Q. Zhang and Z. Chen, "Formation control of multi-agent systems with region constraint," *Complexity* **2019**, 6 (2019), Article ID 8481060. doi: 10.1155/2019/8481060.
28. R. Toyota and T. Namerikawa, "Formation Control of Multi-Agent System Considering Obstacle Avoidance," *2017 56th Annual Conference of the Society of Instrument and Control Engineers of Japan (SICE)* (2017) pp. 446–451.
29. J. Raj, K. Raghuwaiya, J. Vanualailai and B. Sharma, "Path Planning of Multiple Mobile Robots in a Dynamic 3d environment," **In:** *Advances in Computer, Communication and Computational Sciences* (S. K. Bhatia, S. Tiwari, S. Ruidan, M. C. Trivedi and K. K. Mishra, eds.) (Springer, Singapore, 2021) pp. 209–219.
30. X. Yi, J. Wei, D. V. Dimarogonas and K. H. Johansson, "Formation control for multi-agent systems with connectivity preservation and event-triggered controllers**this work was supported by the knut and alice wallenberg foundation, the swedish foundation for strategic research, and the swedish research council," *IFAC-PapersOnLine* **50**(1), 9367–9373 (2017). 20th IFAC World Congress.
31. K. Raghuwaiya, J. Vanualailai and J. Raj, "3D Cylindrical Obstacle Avoidance Using the Minimum Distance Technique," **In:** *Advances in Computer, Communication and Computational Sciences* (S. K. Bhatia, S. Tiwari, S. Ruidan, M. C. Trivedi and K. K. Mishra, eds.) (Springer, Singapore, 2021) pp. 199–208.
32. J. Vanualailai, J. Raj and K. Raghuwaiya, "Autonomous Quadrotor Maneuvers in a 3D Complex Environment," **In:** *Advances in Computer, Communication and Computational Sciences* (S. K. Bhatia, S. Tiwari, S. Ruidan, M. C. Trivedi and K. K. Mishra, eds.) (Springer, Singapore, 2021) pp. 221–231.
33. J. Raj, K. Raghuwaiya, S. Singh, B. Sharma and J. Vanualailai, "Swarming Intelligence of 1-Trailer Systems," **In:** *Advanced Computer and Communication Engineering Technology* (H. A. Sulaiman, M. A. Othman, M. F. I. Othman, Y. A. Rahim and N. C. Pee, eds.) (Springer International Publishing, Cham, 2016) pp. 251–264.
34. C. de Saxe and D. Cebon, "Estimation of trailer off-tracking using visual odometry," *Vehicle Syst. Dyn.* **57**(5), 752–776 (2019).
35. A. Prasad, B. Sharma and J. Vanualailai, "A Geometric Approach to Motion Control of a Standard Tractor-Trailer Robot," *2016 3rd Asia-Pacific World Congress on Computer Science and Engineering (APWC on CSE)* (2016) pp. 53–59.
36. M. Michalek, "Non-minimum-phase property of n-trailer kinematics resulting from off-axle interconnections," *Int. J. Control* **86**(4), 740–758 (2013).
37. A. W. Divelbiss and J. Wen, "A path space approach to nonholonomic motion planning in the presence of obstacles," *IEEE Trans. Robot. Autom.* **13**(3), 443–451 (1997).
38. P. Bolzern, R. M. DeSantis and A. Locatelli, "An input-output linearisation approach to the control of an *n* body articulated vehicle," *J. Dyn. Syst. Meas. Control* **123**(3), 309–316 (2001).
39. M. K. J.-H. Lee, W. Chung and J. Song, "A passive multiple trailer system with off-axle hitching," *Int. J. Control Autom. Syst.* **2**(3), 289–297 (2004).
40. E. Kayacan, H. Ramon and W. Saeys, "Robust trajectory tracking error model-based predictive control for unmanned ground vehicles," *IEEE/ASME Trans. Mechatron.* **21**(2), 806–814 (2016).
41. X. Ding, Y. He, J. Ren and T. Sun, "A Comparative Study of Control Algorithms for Active Trailer Steering Systems of Articulated Heavy Vehicles," *Proceedings of the American Control Conference* Montreal, Canada (2012) pp. 3617–3622.
42. A. Astolfi, P. Bolzern and A. Locatelli, "Path-tracking of a tractor-trailer vehicle along rectilinear and circular paths: A Lyapunov-based approach," *IEEE Trans. Robot. Autom.* **20**(1), 154–160 (2004).
43. O. Elhaki and K. Shojaei, "Observer-based neural adaptive control of a platoon of autonomous tractor-trailer vehicles with uncertain dynamics," *IET Control Theory Appl.* **14**(14), 1898–1911 (2020).
44. J. Liu, X. Dong, J. Wang, O. Ljungqvist, C. Lu, X. Zhao and X. Wang, "A novel EPT autonomous motion control framework for an off-axle hitching tractor-trailer system with drawbar," *IEEE Trans. Intell. Vehicles*, (2020). doi: 10.1109/TIV.2020.3033115.

45. L. Guevara, M. M. Michałek and F. Auat Cheein, "Headland turning algorithmization for autonomous n-trailer vehicles in agricultural scenarios," *Comput. Electron. Agricul.* **175**, 105541 (2020).
46. A. Prasad, B. Sharma and J. Vanualailai, "A solution to the motion planning and control problem of a car-like robot via a single-layer perceptron," *Robotica* **32**(6), 935–952 (2014).
47. A. Prasad, B. Sharma and J. Vanualailai, "A new stabilizing solution for motion planning and control of multiple robots," *Robotica* **34**(5), 1071–1089 (2016).
48. M. Esfandyari, M. A. Fanaei and H. Zohreie, "Adaptive fuzzy tuning of PID controllers," *Neural Comput. Appl.* **23**(1), 19–28 (2013).
49. B. Sharma, J. Vanualailai, K. Raghuwaiya and A. Prasad, "New potential field functions for motion planning and posture control of 1-trailer systems," *Int. J. Math. Comput. Sci.* **3**(1), 45–71 (2008).
50. C. W. Reynolds, "Flocks, Herds, and Schools: A Distributed Behavioral Model, in Computer Graphics," *Proceedings of the 14th Annual Conference on Computer Graphics and Interactive Techniques*, New York, USA, vol. 21(4) (1987) pp. 25–34.
51. A. Mogilner, L. Edelstein-Keshet, L. Bent and A. Spiros, "Mutual interactions, potentials, and individual distance in a social aggregation," *J. Math. Biol.* **47**(4), 352–389 (2003).
52. V. Gazi and K. M. Passino, "A class of attractions/repulsion functions for stable swarm aggregations," *Int. J. Control* **77**(18), 1567–1579 (2004).
53. C. W. Reynolds, "Steering Behaviors for Autonomous Characters," *Proceedings of Game Developers Conference* (Miller Freeman Game Group, San Francisco, California, USA, 1999) pp. 763–782.
54. J. Vanualailai, "Stable emergent formations for a swarm of autonomous car-like vehicles," *Int. J. Adv. Robot. Syst.* **16**(5), 1–17 (2019).
55. E. Forgoston and I. B. Schwartz, "Delay-induced instabilities in self-propelling swarms," *Phys. Rev. E* **77**(3), 035203 (2008).
56. A. Wagdy and A. Khamis, "Adaptive group formation in multirobot systems," *Adv. Artif. Intell.* **2013**, 15 (2013), Article ID 692658. doi: 10.1155/2013/692658.